Study of the Short Range Properties of Nucleons at $Q^2 \leq 12$ GeV^2 Using d(e,e'p)n With CLAS12

A Proposal to PAC30

K. Egiyan*, S. Abrhamyan , G. Asryan, N. Dashyan, Y. Gandilyan, N. Gevorkyan*, H. Hakobyan, P.Paremuzyan
Yerevan Physics Institute

S. Boyarinov, V. Burkert, L.Elouadrhiri, M. Ito, M. Mestayer, D. Higinbotham, J-M. Laget, Yu. Sharabyan, S. Stepanyan
Jefferson Lab

L. B. Weinstein*, S.E. Kuhn, and others
Old Dominion University

H. Egiyan, M. Holtrop, L. Zana
University of New Hampshire

K. Griffioen and others
College of William and Mary

and the CLAS COLLABORATION

(Dated: July 7, 2006)

We are proposing to search for two possible QCD phenomena, Point Like Configurations (PLC) in the proton wave function, and modification of (deeply bound) nucleons involved in Short Range Correlations. We will use the exclusive $d(e, e'p)n$ reaction, which is the most understood nucleon knockout reaction. This search will be an extension of the CLAS e6 experiment, which found no evidence for PLC at $Q^2 < 6$ GeV^2 or for nucleon modification (NM) at $Q^2 < 5$ GeV^2. Since both phenomena are expected to be strongly Q^2 dependent, it is logical to continue these investigations at the higher Q^2 region available with the CEBAF 12 GeV upgrade and the CLAS12 detector. The acceptance, resolutions and projected luminosity of CLAS12 are well suited for the proposed measurements. 32 beam time days will allow us to extend the PLC search up to $Q^2 = 12$ GeV^2, and the MN search up to $Q^2 = 10$ GeV^2 with high statistical precision.

* spokesperson

Contents

I. INTRODUCTION

QCD, the theory of strong interaction, successfully describes hadronic matter at asymptotic short distances. However, QCD still fails to describe real hadronic matter, such as nucleons and nuclei. The logical physics challenge is to study real hadronic matter at shorter and shorter distances, in order to discover at what distances QCD can describe it. QCD arguments predict two phenomena in the Short Range (distances less than the nucleon radius) Properties of nucleons: 1) the existence of Point-Like Configurations (PLC) and 2) the modification (eg: size, form factors, quark distributions) of deeply bound nucleons involved in Short Range Correlated (SRC) nucleon pairs.

We will search for these phenomena using the simplest nucleus, deuterium, as a micro-laboratory. We will use deuterium for two reasons. 1) SRC appear to be the same in all nuclei[1] and 2) deuterium has the best known WF and offers the best possible interpretation of the experimental data. Therefore we will study the $d(e, e'p)n$ reaction

$$e + d \rightarrow e' + p + n \tag{1}$$

In order to reduce systematic uncertainties, both experimental and theoretical, we will construct ratios of $d(e, e'p)n$ cross sections. We will typically construct the ratio of the cross section where we expect the PLC (or NM) effect to be large to the cross section where we expect the PLC (or NM) effect to be negligible. We will do this for both experimental and theoretical cross sections and then construct the double ratio of the experimental to theoretical ratios.

We will follow the analysis procedures of the CLAS e04019 measurement[2, 3] (part of the e6 run group), where we first validated the theoretical model by comparing to measured cross sections, and then searched for PLC and NM using ratios of cross sections. This experiment did not find any evidence for PLC up to $Q^2 = 6$ GeV^2 or for NM up to $Q^2 = 5$ GeV^2. A parallel measurement looking at backward spectator protons[4] also found no evidence for PLC. Therefore, it is crucial to extend these studies to higher Q^2.

The proposed experiment will study the exclusive $d(e, e'p)n$ reaction up to recoil momentum $p_n = 650$ MeV/c and $Q^2 = 12$ GeV^2 using an 11 GeV electron beam, CLAS12, and 32 days of beam time.

II. MOTIVATION

Current NN interaction models, while tightly constrained by the large body of NN elastic scattering data, do not explicitly account for the quark-gluon substructure of the interacting nucleons. Indeed, it is an open question whether this rich substructure is correctly and/or adequately represented in these models at short internucleon separations. It is also unclear whether the short range structure in nuclei implied by these interactions is correct. The deuteron, being the simplest nucleus, is the nucleus of choice for carrying out the systematic study of these issues, with the possibility of extending these measurements at high momentum transfer and missing momentum to other few-body systems (eg: $A = 3$ and 4) amenable to accurate calculations.

One fascinating question in nuclear physics is at what level does the quark-gluon picture supersede the nucleon-meson picture? Clearly, when the wave functions of the two nucleons overlap significantly, one can expect large changes in the internal structure of the nucleons. This may lead to a change in form factors or structure functions (depending on the off-shell mass, m^*, of the struck nucleon) or, in the extreme case, to a complete fusion of the two nucleons into a six-quark object. The chance of significant nucleon overlap occurring is quite high. The

probability of finding a nucleon inside the nucleus in a short range correlation (ie: at momentum greater than 275 MeV/c and with that momentum balanced by the momentum of only one other nucleon) is 25% in heavy nuclei and 4% in deuterium.[1] By designing experiments that are sensitive to short range correlations (SRC) in nuclei, we can amplify the effects of QCD (ie: quark-gluon) degrees of freedom. We will use the simplest nucleus, deuterium, for which the interpretation of the data is easiest and realistic calculations exist.

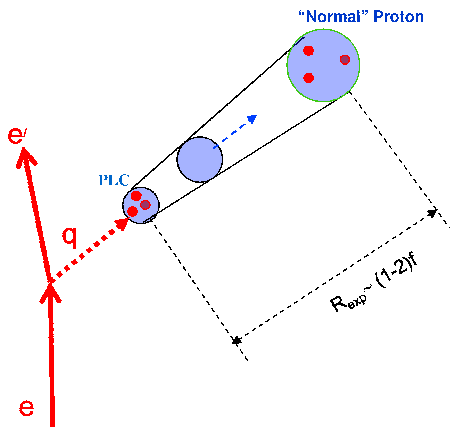

FIG. 1: The evolution of a struck proton from a PLC back to a 'normal' (ie: unmodified) proton.

We will search for two specific QCD degrees of freedom

- Point-Like Configurations (PLC) in the nucleon
- Modification of deeply bound nucleons

Point-Like Configurations (PLC) in the nucleon. QCD predicts that in hard elastic electron-nucleon scattering, a small color-singlet object can be produced, which is also called a Point-Like Configuration [5, 6]. Due to its small size, the PLC should interact in the medium with a lower cross section than the unmodified proton. It will also expand as it propagates. The expansion length, R_{exp}, depends strongly on Q^2 and is believed to be about $R_{exp} \approx 1 - 2$ fm. See Fig. 1. The problem lies in experimentally identifying the PLC.

The general method for searching for PLC is by looking for the expected reduced cross section for the PLC interaction with the nuclear medium (in this case, with the residual neutron). By choosing Q^2 such that the expansion length is larger than the deuteron radius, $R_{exp} > R_{deut}$, the struck PLC should remain a PLC until it has exited the nucleus. In this case, it will have a smaller Final State Interaction cross section than the free NN cross section (see Fig. 2).

One way to look for this reduced reinteraction cross section is to calculate the ratio of the observed experimental cross section, σ_{exp}, (which of course includes FSI effects) to the calculated theoretical cross section without FSI, σ_{the}^{PW}:

$$T_{e/t}(Q^2, p_n) = \frac{\sigma_{exp}(Q^2, p_n)}{\sigma_{the}^{PW}(Q^2, p_n)} \tag{2}$$

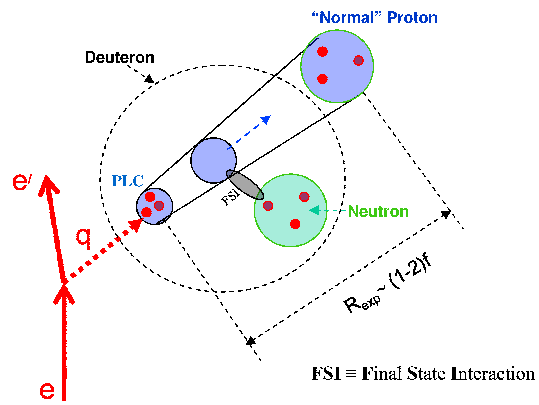

FIG. 2: The reduced Final State Interaction of a PLC.

where p_n is the neutron recoil momentum. Ideally, if PLC become more important with Q^2, then this ratio should tend toward unity as Q^2 increases (at fixed p_n). Unfortunately, this method requires low systematic uncertainties in both the experimental and theoretical cross sections. Since the expected effect for deuterium is quite small, this method is impractical.

Rather then calculating the transparency as the ratio of experiment to theory, $T_{e/t}$, which suffers from both experimental and theoretical uncertainties, we will measure the purely experimental ratio

$$T_{e/e}(Q^2) = \frac{\sigma_{exp}^{FSI}(Q^2)}{\sigma_{exp}^{NFSI}(Q^2)} \tag{3}$$

of σ_{exp}^{FSI}, the cross section in a kinematic region where FSI **do** contribute significantly, to σ_{exp}^{NFSI}, the cross section in a kinematic region where FSI do not contribute significantly. We will compare this experimental ratio to the similar theoretical ratio $T_{t/t}$.

$$T_{t/t}(Q^2) = \frac{\sigma_{the}^{FSI}(Q^2)}{\sigma_{the}^{NFSI}(Q^2)} \tag{4}$$

(Note that FSI and $NFSI$ refer to kinematic regions where FSI are expected to be important and unimportant, respectively.)

In the double ratio, $T_{e/e}(Q^2)/T_{t/t}(Q^2)$, most of the experimental and theoretical uncertainties should drop out. We will look at the behavior of this double ratio as a function of Q^2 to look for PLC in nuclei.

There are theoretical estimations for PLC effects. In [6] the $d(e, e'p)n$ reaction is studied in perpendicular kinematics ($x_B = 1$) to obtain evidence of PLC existence. They show that the sensitivity of this reaction to PLC depends strongly on the recoil neutron's momentum p_n. Fig. 3 shows the Q^2 dependence of T (equivalent to the experiment-theory ratio of Eq.2) for 5 values

of p_n. One can see that in some cases (at $0.1 < p_n < 0.3$ GeV/c and $p_n > 0.4$ GeV/c) the PLC effect is expected to be more than 10% for $5 < Q^2 < 6$ GeV^2. In [15] the new calculations were carried out in slightly different kinematics, $\alpha = 1$ (where $\alpha_n = \frac{E_n - p_n \cos\theta_{\gamma n}}{m_n}$). Again, as one can see from Fig.4 there is a 10–15% effect expected at $5 < Q^2 < 6$ GeV^2.

However, in existing experimental data such a big effect was not obtained. These experimental data (from CLAS, Hall C and SLAC) will be discussed in a section RESULTS.

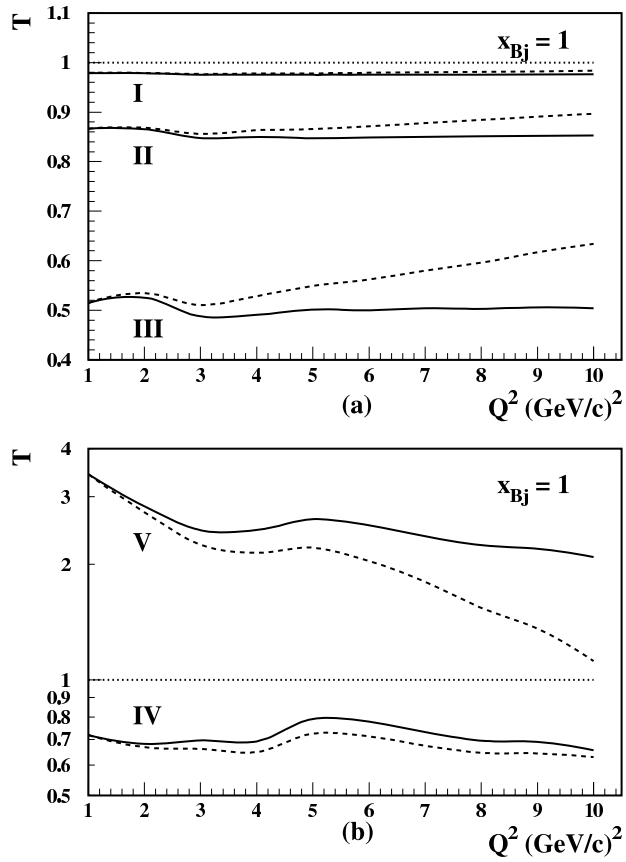

Fig.3

FIG. 3: The transparency (ratio of experimental to theoretical PWIA cross sections) calculated for $p_n = 0, 100, 200, 300$ and 400 MeV/c (curves I – V respectively) as a function of Q^2 at $x_B = 1$ [6]. The solid lines are the glauber calculations and the dashed lines include the effects of color transparency.

Modification of deeply bound nucleons. The second QCD degree of freedom that we will search for is modification of deeply bound nucleons. Nuclei are not bags of independent nucleons. The attractive and repulsive components of the NN potential lead to the creation of short range correlations (SRC), in which two nucleons have large relative momenta ($p > 300$ MeV/c). There is a $4 \pm 0.8\%$ probability that the nucleons in deuterium are in an SRC [1]. The nucleons in

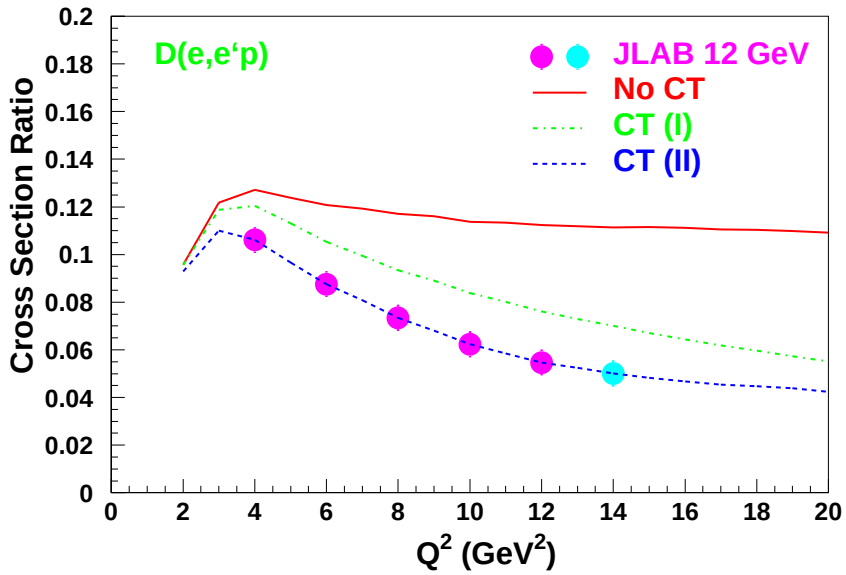

FIG. 4: The ratio of the experimental cross sections at $p_n = 400$ and 200 MeV/c as a function of Q^2 at $\alpha = 1$ [15]. The solid red curve has no color transparency (ie: PLC) effects. The green and blue curves use different CT models.

an SRC are at very small distances and therefore overlap significantly. This overlap of deeply bound nucleons is expected to cause them to be modified.

There have been many previous searches for nucleon modification in nuclei. These have been complicated by theoretical uncertainties in the reaction mechanism, especially in two-nucleon currents and final state interactions. Unpolarized $A(e, e')$ experiments with light and medium nuclei observed a change in the ratio of longitudinal and transverse response functions relative to free protons. Unpolarized $A(e, e'p)$ measurements [7–9] showed that most of this effect occurred at missing energies greater than the two-nucleon knockout threshold, indicating that the extra transverse cross section was due to two-nucleon currents (eg: Meson Exchange Currents (MEC) and Isobar Configurations(IC)). The deviation of the L/T ratio at lower missing energies was eventually explained in terms of FSI effects.[10]

The best evidence for nucleon modification comes from a ^{4}He$(\vec{e}, e'\vec{p})$ measurement of the double ratio of the tranverse (P'_x) and longitudinal (P'_z) polarization transfer for ^{4}He relative to the proton:

$$R = \frac{(P'_x/P'_z)_{^4\mathrm{He}}}{(P'_x/P'_z)_{^1\mathrm{H}}} \tag{5}$$

This double ratio has been measured to be approximately 90% of the same ratio calculated in Plane Wave Impulse Approximation (PWIA).[11] This cannot be explained by relativistic Distorted Wave Impulse Approximation (DWIA) calculations without including nucleon modification. However, more recent calculations[12] which include MEC and charge exchange FSI can explain the data without invoking nucleon modification.

All these searches for nucleon modification are indirect and at low momentum transfers,

where FSI effects are hard to suppress. Therefore, the problem is still unsolved.

We will study this problem in a much more direct way. In order to search for nucleon modification, we will study the Q^2 dependence of electron scattering from a deeply bound proton in a NN SRC in deuterium (Fig.5).

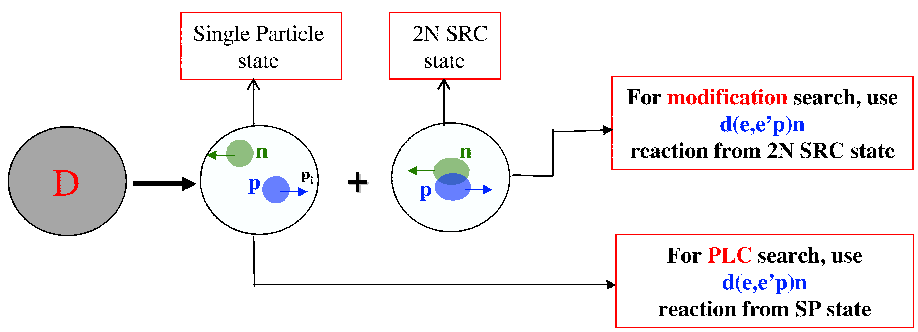

FIG. 5: The two components of deuterium WF, for PLC and Nucleon Modification searches.

To do that, we need to separate from the measured experimental cross section the component proportional only to the deuterium wave function, by suppressing the FSI contribution. The standard way to do this is to go to parallel or antiparallel kinematics (where the neutron recoils parallel or antiparallel to the virtual photon direction). This is not feasible in CLAS due to low luminosity. We will instead suppress FSI by looking at backward production kinematics, where the neutron is emitted in the backward direction relative to the virtual photon. We will find a value of the light cone variable

$$\alpha_n = \frac{E_n - p_n \cos\theta_{\gamma n}}{m_n} \tag{6}$$

such that for $\alpha_n > \alpha_0$, the experimental cross section is equal to the theoretical cross sections both with and without FSI:

$$\sigma_{exp} = \sigma_{PWIA} = \sigma_{FSI}(full) \tag{7}$$

Ref. [14] shows that by choosing $\alpha_0 = 1.23$, the FSI contribution can be suppressed in the neutron momentum interval $450 < p_n < 650$ MeV/c. On the other hand, there is another momentum range $p_n < 100$ MeV/c where there is also no FSI contribution. Thus, in both momentum regions, the recoil neutrons are spectators. On the other hand, there are differences in the nucleon states in the two regions. At low momenta, $p_n < 100$ MeV/c, nucleons are not deeply bound and we do not expect them to be modified, while at higher momentum, $450 < p_n < 650$ MeV/c, the nucleons are deeply bound, and we expect them to be modified. We will construct the two ratios

$$R_{exp}(Q^2) = \frac{\sigma_{exp}^{0.55}(Q^2)}{\sigma_{exp}^{<0.1}(Q^2)} \tag{8}$$

and

$$R_{PW}(Q^2) = \frac{\sigma_{PW}^{0.55}(Q^2)}{\sigma_{PW}^{<0.1}(Q^2)} \tag{9}$$

where $\sigma_{exp}^{0.55}(Q^2)$ and $\sigma_{exp}^{<0.1}(Q^2)$, and $\sigma_{PW}^{0.55}(Q^2)$ and $\sigma_{PW}^{<0.1}(Q^2)$ are the experimental and PWIA theoretical integrated cross sections in the two corresponding momentum intervals. If $R_{PW}(Q^2)$ is calculated with the same proton formfactor in both neutron momentum intervals, then by looking at the difference between the Q^2 dependences of $R_{exp}(Q^2)$ and $R_{PW}(Q^2)$, we hope to find a signature for modification of the deeply bound proton.

III. EXPERIMENT

A. CLAS12 acceptances and resolution acceptablility for the proposed studies.

This experiment will use the standard CLAS12 detectors at the full design luminosity of $\mathcal{L} = 2.10^{35}$ cm^{-2}s^{-1}. The primary questions to be resolved are a) the ability to determine the exclusive final state of the $d(e, e'p)n$ reaction, b) the neutron momentum resolution, and c) the angular coverage.

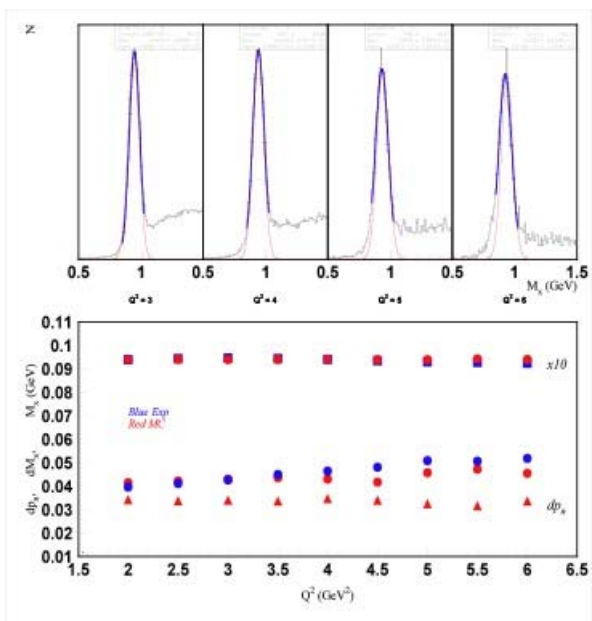

FIG. 6: (top) The observed missing mass distribution for $d(e, e'p)X$ for CLAS e6 data for different Q^2 bins. The histogram is the data and the red curve is the simulation of the $d(e, e'p)n$ reaction, (bottom) Neutron mass centroid (M_m) and width (dM_m) and neutron momentum resolution (dp_n) for data (blue squares) and simulation (red triangles).

Determining the exclusive $d(e, e'p)n$ final state. Separation of the exclusive final state of the $d(e, e'p)n$ reaction from the other $d(e, e'p)X$ channels will be done, as it was done in the CLAS e6 experiment, by measuring the recoil neutron missing mass. The histograms in the top panel of Fig.6 show the missing mass distributions from CLAS e6 data for four Q^2 bins. The exclusive final state contributions are concentrated under the peaks. For correct measurements

of cross sections, the background under the peaks should be subtracted in every measured cross section distribution, in every kinematic bin. For the CLAS e6 experiment this was done very carefully, achieving corresponding systematic uncertainties less than 5% [14]. The background level depends strongly on missing mass resolution. The CLAS e6 neutron mass resolution as a function of Q^2 is shown in the bottom panel by the blue squares. The corresponding Monte Carlo simulation of the missing mass distributions can be seen also in Fig. 6 [14]. The width and location of the neutron mass peak is well reproduced by the simulation. Note that sinulations were carried out with the CLAS standard resolutions listed in Ref. [13], at a Torus magnet current of 2250 A.

The neutron momentum resolution. Accurate knowledge of the neutron momentum resolution is important since the $d(e, e'p)n$ reaction will be studied using the neutron momentum and angular distributions (ie: by choosing kinematics where the proton absorbs the virtual photon and the neutron's final state momentum is related to its initial momentum in the nucleus). The $d(e, e'p)n$ reaction study with the proton momentum and angular distributions is unacceptable, because we cannot detect protons with $p_p < 300$ MeV/c and therefore we cannot study the deuterium wave function in this important region. This can be seen from Fig. 7. Due to the CLAS threshold in proton detection, there is momentum cut at ≈ 300 MeV/c, while in neutron spectra this regions are available to use.

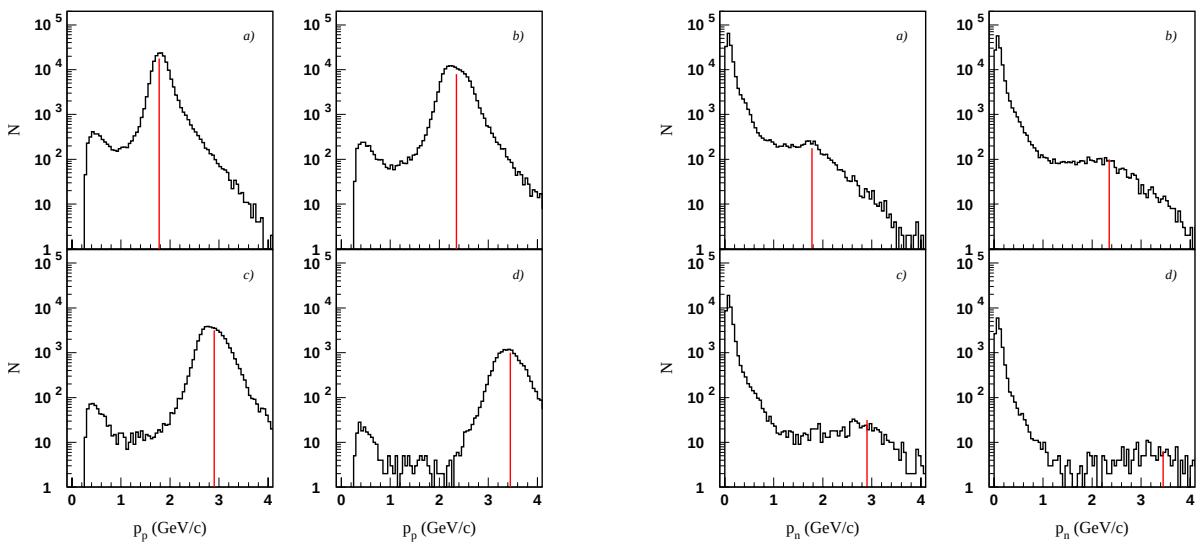

FIG. 7: (left) Proton momentum distributions. a), b), c) and d) for $Q^2 = 2, 3, 4$ and 5 GeV^2. (right) The same for neutrons. Vertical lines indicate the elastic (eN) scattering peak position.

In Fig.6 the simulated neutron momentum resolutions are shown by the red triangles. The average resolution is 35 MeV/c. This is a little smaller than the width obtained from the measured H$(e, e'p)$ missing momentum resolution of 41 MeV/c.

Proposed measurements with CLAS12 will be carried out with the same technique. The similar simulation results on missing mass resolutions for CLAS12 are shown in Fig. 8. The left panel shows the neutron mass resolution, assuming the electron and proton resolutions listed in the Conceptual Design Report:

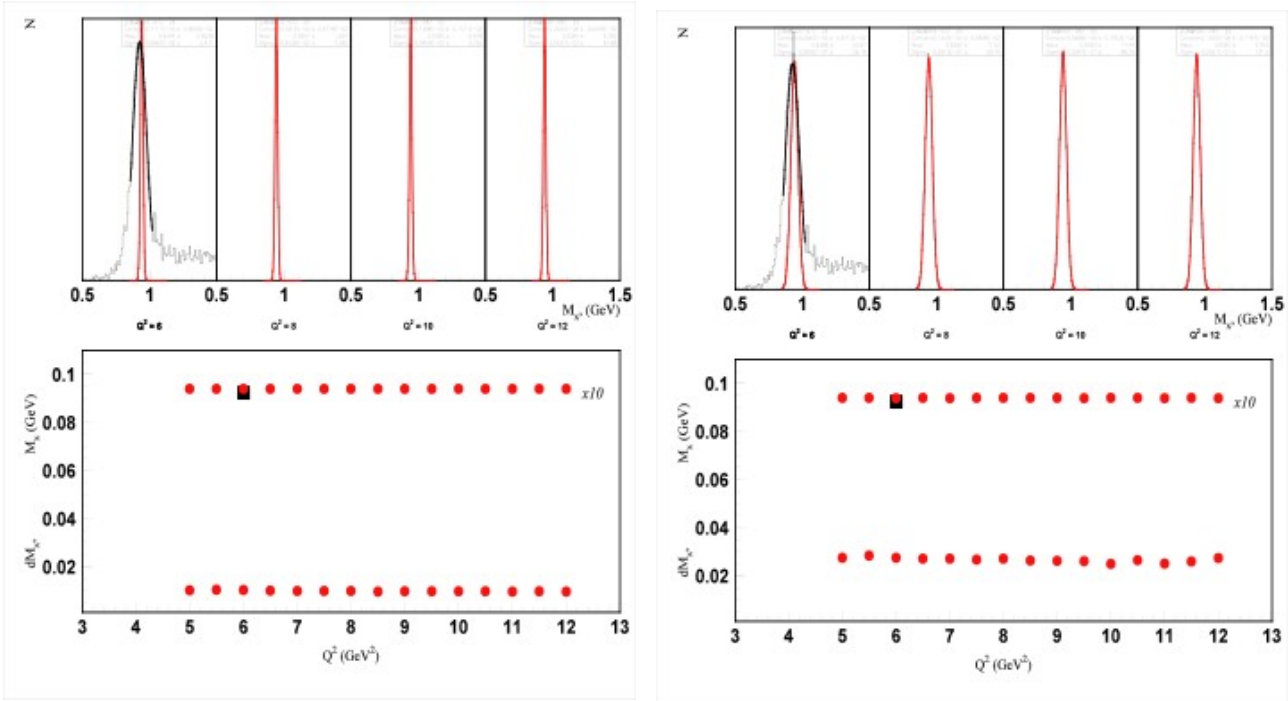

FIG. 8: (top) Missing mass distribution for $d(e, e'p)X$ for CLAS e6 data at $Q^2 = 6$ GeV^2 and for simulated CLAS12 data at $6 \leq Q^2 \leq 12$ GeV^2. (bottom) Neutron mass centroid (M_m) and width (dM_m). The red circles are the CLAS12 simulation and the blue square at $Q^2 = 6$ GeV^2 is from e6 data. The left plots are for the nominal CLAS12 resolutions and the right plots are for nominal angular resolutions and an increased intrinsic momentum resolution of 0.3%.

- Polar angle resolution $\sigma_\theta \approx 1$ mr
- Azimuthal angle resolution $\sigma_\phi \approx 4$ mr
- Momentum resolution
  - Forward angle: $\sigma_p/p = \sqrt{(0.1\%)^2 + (0.2\%/\beta)^2}$
  - At 90° and $p = 1$ GeV: $\sigma_p/p = 2.2\%$

The right side of Fig. 8 shows the neutron mass resolution if the intrinsic momentum resolution of the electron and proton is increased from 0.1 to 0.3%. For the nominal momentum resolution of 0.1%, the expected neutron mass resolution is about 10 MeV and therefore we expect that the neutron momentum resolution will be better than 10 MeV/c. For the decreased momentum resolution of 0.3%, the expected neutron mass and momentum resolutions will be about 30 MeV and 30 MeV/c respectively.

The angular coverage of the CLAS12 detector will also be well suited for the proposed studies. The PLC studies will concentrate on $\alpha_n = 1 \pm 0.1$, the region where FSI are expected to be maximum (see below). They will look at a range of neutron momenta from 0 to 0.6 GeV/c. Fig. 9a shows the range of electron angles as a function of Q^2 for the e6 data and for the proposed 11 GeV measurement at $\alpha_n = 1 \pm 0.1$ and $0.4 \leq p_n \leq 0.6$ GeV/c. Note that the electron angles will all be within the acceptance of the forward detector. Fig. 9b shows the range of proton

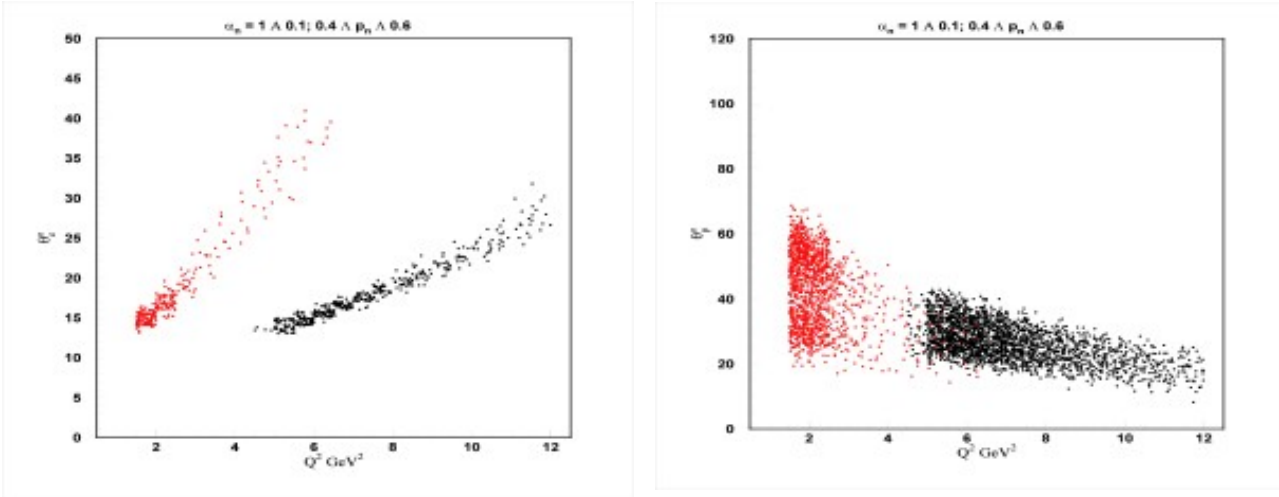

FIG. 9: (left) Electron scattering angle vs Q^2 for $\alpha_n = 1 \pm 0.1$ and for $0.4 \leq p_n \leq 0.6$ GeV/c, the kinematics of the PLC studies, for the E6 data and for the expected 11 GeV data. (right) Proton angle vs Q^2 for the same kinematics.

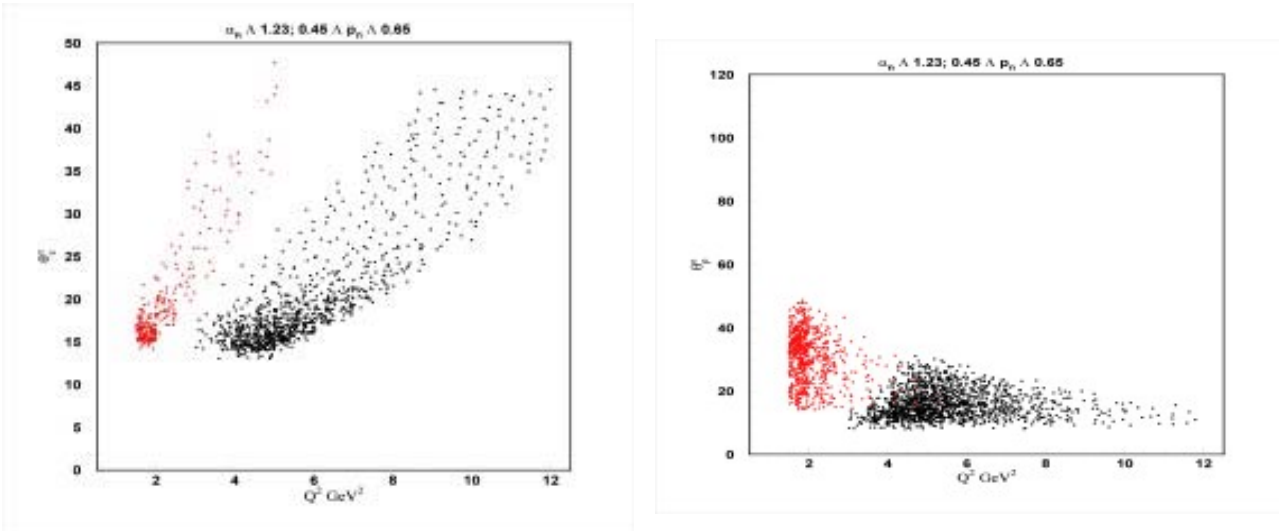

FIG. 10: (left) Electron scattering angle vs Q^2 for $\alpha_n > 1.23$ and for $0.45 \leq p_n \leq 0.65$ GeV/c, the kinematics of the nucleon modification studies, for the E6 data and for the expected 11 GeV data. (right) Proton angle vs Q^2 for the same kinematics.

angles as a function of Q^2 for the e6 data and for the proposed 11 GeV measurement. The 11 GeV proton angles will also all be within the acceptance of the forward detector (although the e6 proton angles would not have been).

The nucleon modification studies will concentrate on $\alpha_n > 1.23$, where the backward going neutron is least affected by FSI. Fig. 10 shows the ranges of electron and proton angles as a function of Q^2 for $\alpha_n > 1.23$ and $0.455 \leq p_n \leq 0.65$ for the e6 data and for the expected 11

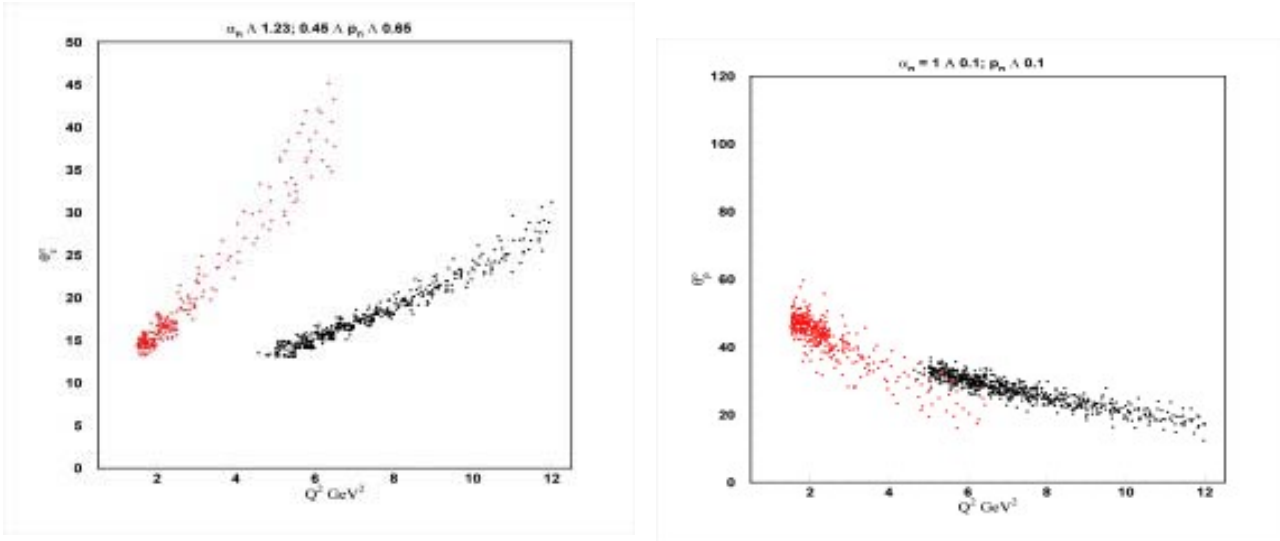

FIG. 11: (left) Electron scattering angle vs Q^2 for $\alpha_n = 1 \pm 0.1$ and for $p_n < 0.1$ GeV/c for the E6 data and for the expected 11 GeV data. (right) Proton angle vs Q^2 for the same kinematics.

GeV measurement. Note that there is some loss of electron acceptance at the largest Q^2, but that the protons will all be within the angular acceptance of the forward detector.

Both the nucleon modification and the PLC studies will rely on calculating the ratio of the cross section in the region where we hope to find these exotic phenomena to the cross section in the region $p_n < 0.1$ GeV/c where we expect the standard hadronic degrees of freedom to dominate. Fig. 11 shows the electron and proton angular ranges for $\alpha_n = 1 \pm 0.1$ and $p_n < 0.1$ GeV/c for the e6 data and the expected 11 GeV measurement. The electrons and protons will both be detected in the forward detector.

Thus, we expect that the experimental acceptances and resolutions will be quite acceptable for the proposed studies.

B. Experimental Measurements

Both searches, for PLC and for nucleon modification, are looking for variations of the neutron momentum and polar angle in the $d(e, e'p)n$ reaction. Therefore, we will first measure the momentum and angular distributions, and show that these data are correct and reasonable, *i.e.* that the mechanism of the $d(e, e'p)n$ reaction is well understood. We will compare measured data with model calculations of the $d(e, e'p)n$ reaction.

Specifically, we will use Jean-Marc Laget's model based on his diagramatic approach [16]. The model is an extension of earlier diagrammatic methods [17, 18] to JLab kinematics. Four main amplitudes contribute in these calculations (see Fig. 12),

1. Plane Wave Impulse Approximation (PWIA) where the virtual photon is absorbed by the proton and the neutron is a spectator,

2. Meson Exchange Currents (MEC) where the virtual photon is absorbed by a meson exchanged between the two nucleons,

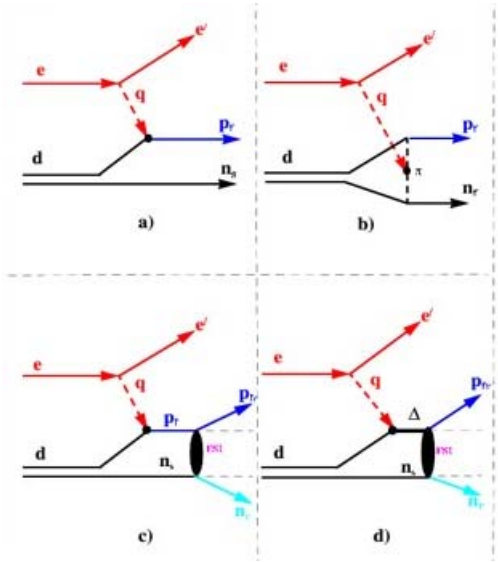

FIG. 12: $d(e, e'p)n$ reaction mechanisms: a) PWIA, b) MEC, c) FSI, d) Isobar Configuration ($\Delta N \rightarrow NN$ FSI).

3. Final State Interactions (FSI) where the virtual photon is absorbed by one nucleon and that nucleon rescatters from the other nucleon via high energy diffractive nucleon-nucleon elastic scattering, and

4. Isobar Configurations (IC) where the virtual photon is absorbed on one nucleon, exciting it to a Δ, which deexcites by rescattering from the other nucleon.

Deuteron wave functions derived from both the Paris [19] and the Argonne V18 potentials were used. The electron couples to the nucleons through a fully relativistic, on-shell nucleon current. The dipole parameterization was chosen for the magnetic form factors of the nucleon. The latest JLab data [20] were used for the proton electric form factor, while the Galster [21] parameterization was selected for the neutron electric form factor. The parameters of the NN amplitude are the same as in Ref. [16], and are fixed by the elastic scattering cross section. The π and ρ exchanges are taken into account in the MEC and ΔN formation amplitudes, as described in Ref. [18]. The electromagnetic $N \rightarrow \Delta$ transition form factor $F_{N\Delta}(Q^2) = (1 - Q^2/9)/(1 + Q^2/0.7)^2$ is driven by the world data and specifically by the highest Q^2 measurement [22] in Hall C at JLab. The most recent data set [23] from CLAS is lower by as much as 10% for $Q^2 < 3$ GeV^2 but is similar for $Q2 > 3$ GeV^2.

Laget's model has been compared with existing e6 CLAS data to demonstrate that we have a good understanding of the $d(e, e'p)n$ reaction mechanism.

In order to compare with CLAS data, Laget's model has been programmed into a Monte-Carlo code that generates events in the fiducial acceptance of CLAS. We sampled p_n, θ_n, ϕ_n (the azimuthal angle of the neutron around the momentum transfer direction), ϕ_e (the azimuthal angle of the scattered electron) and $Q2$ from a flat distribution, and then calculated all remaining momenta and angles constrained by quasi-elastic kinematics. If the electron and the proton fell in the CLAS acceptance we recorded the kinematics of the event in a database (namely a PAW Ntuple) and weighted it with the corresponding cross section, differential in $p_n, \theta_n, \phi_n, Q2$ and ϕ_e . The events were then binned identically to the experimental data using the same cuts.

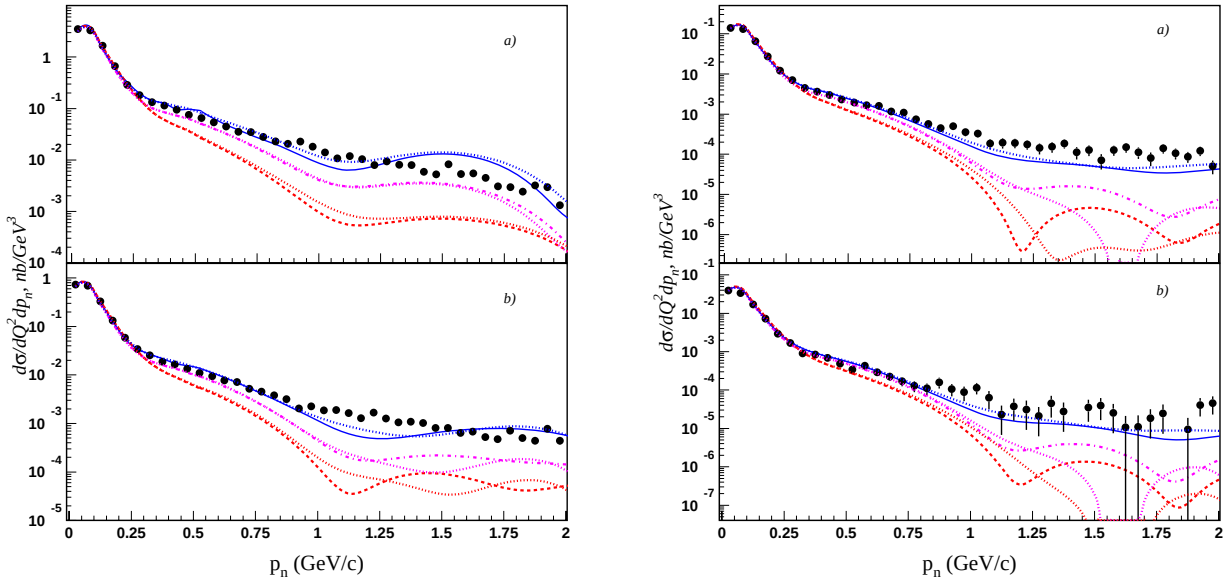

FIG. 13: $d(e,e'p)n$ reaction cross section vs neutron momentum in CLAS at $Q^2 = 2,3,4$ and 5 GeV^2 (increasing from upper left to lower right). The red (lowest) curves are PWIA, the magenta (intermediate) curves also include FSI, and the blue (highest) curves also include IC. The two curves for each reaction mechanism use the Paris and AV18 potentials.

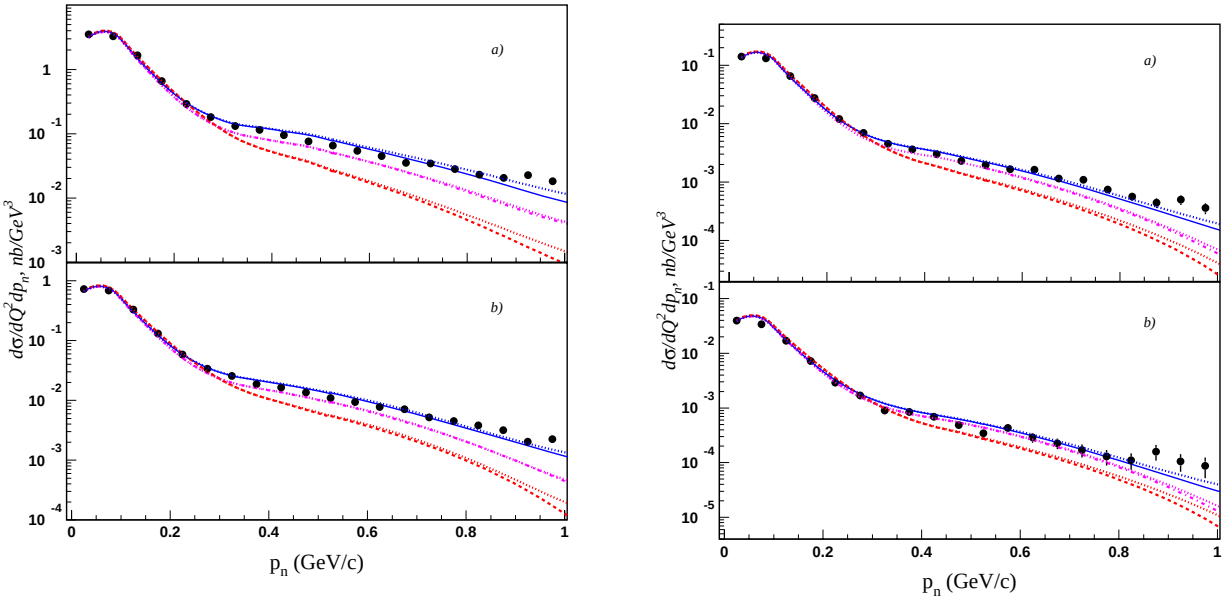

FIG. 14: $d(e,e'p)n$ reaction cross section vs neutron momentum in CLAS at $Q^2 = 2,3,4$ and 5 GeV^2 with expanded horizontal scale.

No normalization factors between theoretical and experimental data were used.

The comparison between CLAS e6 data and the calculation can be seen in Figs. 13, 14, and 15. Figs. 13 and 14 show the cross section as a function of neutron momentum p_n for four bins of Q^2. The data and the calculation are integrated over the other kinematic variables within the CLAS acceptance. The data and the full calculation agree well up to $p_n \approx 1$ GeV/c. For $p_n < 0.25$ GeV/c, the PWIA calculation describes the data very well. Above 0.25 GeV/c, NN elastic FSI become important and above 0.75 GeV/c IC become important. The Paris and AV18 PWIA calculations agree up to about 0.75 GeV/c, indicating that the wave function is well constrained up to that point. We will restrict ourselves to comparisons at $p_n < 0.75$ GeV/c.

Although the theory describes the neutron momentum distributions well, the log scale makes a close comparison difficult. The differences between theory and experiment are best seen quantitatively in the linear plots of angular distributions for various regions in p_n below 750 MeV/c. In Refs. [24, 25] it has been shown that there are specific features of recoil neutron angular distributions for $p_n < 0.1$ GeV/c (the angular distributions are expected to be insensitive to FSI), $p_n \sim 0.4 - 0.5$ GeV/c (FSI should dominate) and $0.2 < p_n < 0.3$ GeV/c (the interference between the PWIA and FSIs amplitudes should contribute).

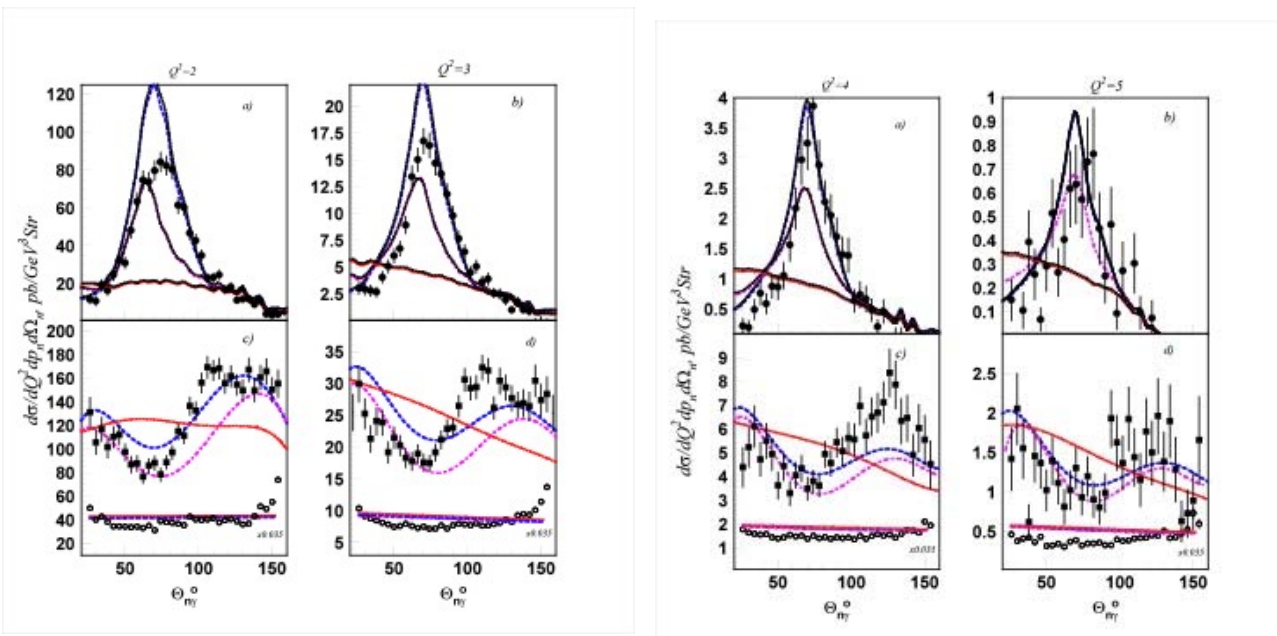

FIG. 15: $d(e, e'p)n$ reaction cross section vs neutron-virtual photon angle for three neutron momentum ranges at $Q^2 = 2, 3, 4$ and 5 GeV^2 (increasing from left to right). The red (lowest) curves are PWIA, the magenta (intermediate) curves also include FSI, and the blue (highest) curves also include IC. The upper panel for each Q^2 shows the data for $0.4 < p_n < 0.6$ GeV/c and the lower panel shows the data for $p_n < 0.1$ GeV/c (lower curve) and for $0.2 < p_n < 0.3$ GeV/c (upper curve).

We will look specifically at these three neutron momentum ranges. Fig. 15 shows the cross section as a function of θ_{nq}, the neutron-virtual photon angle, for $Q^2 = 2, 3, 4$ and 5 GeV^2 (increasing from left to right) and for the three p_n ranges (increasing from bottom to top). The neutron angular distributions for both the data and the calculation at $p_n < 0.1$ GeV/c are isotropic, as we expect from spectator neutrons (ie: with no FSI).

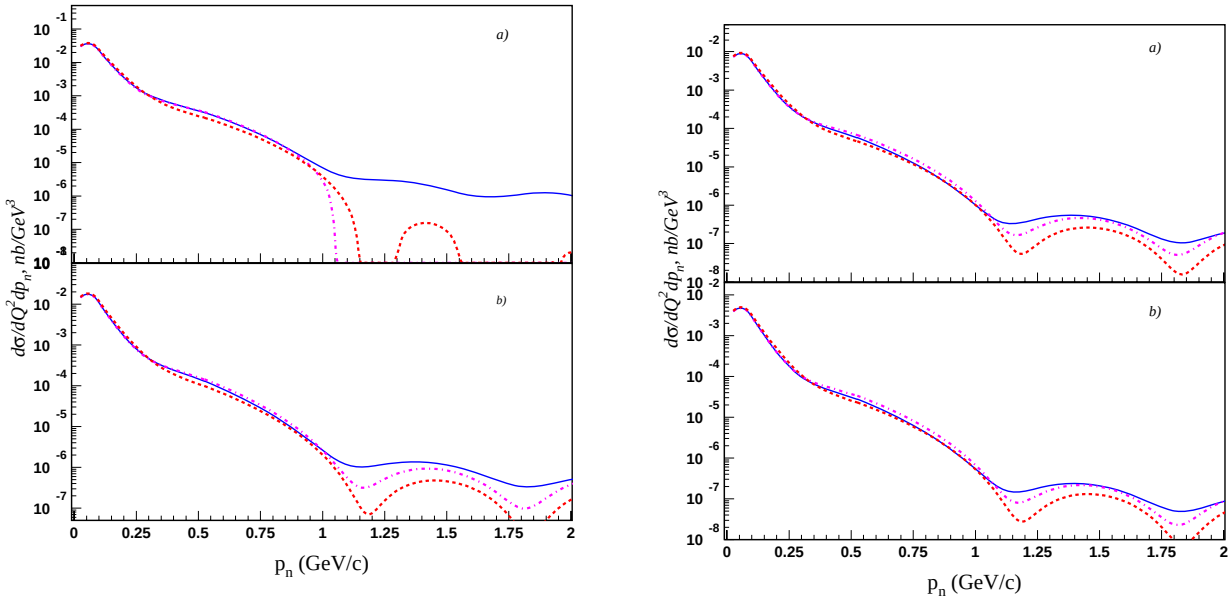

FIG. 16: $d(e,e'p)n$ reaction cross section vs neutron momentum in CLAS12. Left: (a) $Q^2 = 7$, and (b) $Q^2 = 8$, Right: a) $Q^2 = 9$, and (b) $Q^2 = 10$ GeV^2. The red (lowest) curves are PWIA, the magenta (intermediate) curves also include FSI, and the blue (highest) curves also include IC. Calculations are done using the Paris potential in the deuterium WF.

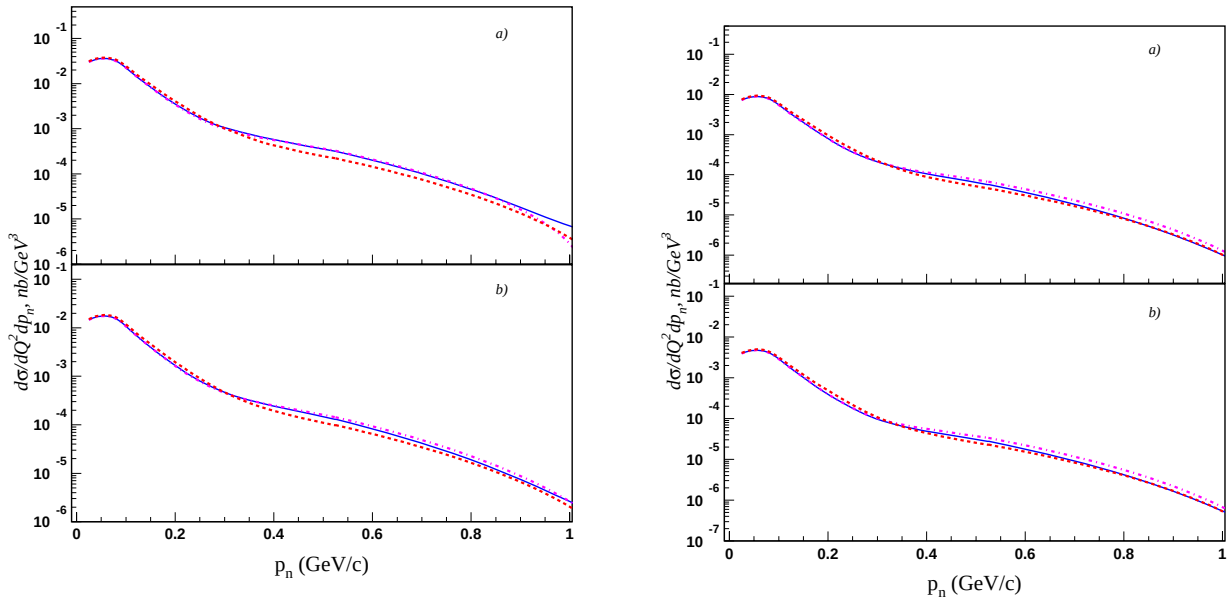

FIG. 17: The same as in Fig.16 with expanded horizontal scale.

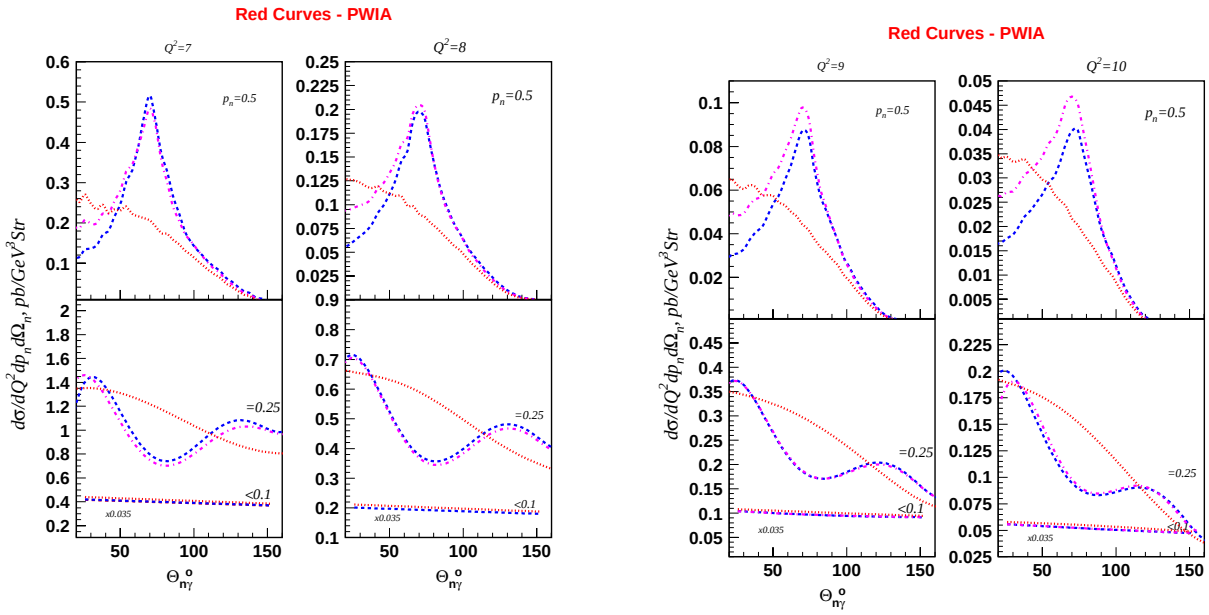

FIG. 18: $d(e,e'p)n$ reaction cross section vs neutron-virtual photon angle in CLAS12 for three neutron momentum ranges ($p_n < 0.1$ GeV/c, $0.2 \leq p_n \leq 0.3$ GeV/c and $0.4 \leq p_n \leq 0.6$ GeV/c) at $Q^2 = 7, 8, 9$ and 12 GeV^2 (increasing from left to right). The red curves are PWIA, the magenta curves also include FSI, and the blue curves also include IC. Calculations are done with the Paris potential in deuterium WF.

The angular distributions for $0.4 < p_n < 0.6$ GeV/c are peaked at about 70°; this implies the dominance of peripheral relativistic rescattering. In Laget's model this comes from neutron-proton rescattering (FSIs), and corresponds to the on-shell propagation of the struck nucleon. It is maximum when the kinematics allow for rescattering on a nucleon almost at rest (i.e.: at $x_B \approx 1$).

The angular distributions at intermediate momenta $0.2 < p_n < 0.3$ GeV/c exhibit a more complex structure, but with a minimum at about 70°, consistent with an interference between FSI and PWIA amplitudes. Note that the full calculation agrees reasonably well with the data.

Theoretical and experimental cross sections agree within 20%, consistent with the systematical uncertainties (≈15% in theoretical calculations and ≈10% in experimental measurements) [14]. Note that there is no normalization between theory and experiment

Thus, the mechanisms of the exclusive $d(e,e'p)n$ reaction are well understood and under control for $1.75 \leq Q^2 \leq 5.5$ GeV^2.

We will check that this understanding of the $d(e,e'p)n$ reaction extends to higher Q^2 ($5 \leq Q^2 \leq 12$ GeV^2) by making the same comparisons between data and theory using data from CLAS12 at a beam energy of 11 GeV. Figs. 16, 17 and 18 show the expected (MC simulated) momentum and angular distributions for $Q^2 = 7, 8, 9$ and 10 GeV^2. One can see that at higher Q^2 the main features of these distributions (especially angular distributions) remain, which will help us to determine our understanding of the mechanism of the $d(e,e'p)n$ reaction. This understanding of the basic reaction mechanism will then allow us to search for the more exotic phenomena of PLC and nucleon modification.

The extrapolation of the theory to 12 GeV is not trivial. Although the rescattering amplitude

is in principle well defined, it relies on our knowledge of the elementary amplitudes in a domain where they have not been determined yet. In the NN sector the angular distributions and spin observables have been determined up to $T_p = 3$ GeV (Saturne,...) which corresponds to $Q^2 = 6$ GeV^2 (at $x = 1$). Above that, pp scattering is known only at forward angles. The nucleon charge and $N \to \Delta$ electromagnetic form factor has only been determined up to $Q^2 = 6$ GeV^2 and has been extrapolated above that. The magnetic nucleon form factor, which dominates, is known at higher Q^2. Athough we have extrapolated the various electromagnetic form factor above $Q^2 = 6$ GeV^2, one may expect that at the time when the experiment is performed their actual values will be available (from concurent experiments at JLab12).

IV. RESULTS

This section describes the techniques and expected sensitivities of the proposed search for Point Like Configurations (PLC) and Nucleon Modification (NM) in deuterium and the results of previous searches using the same technique.

A. Previous searches for PLC

As discussed in the Motivation section, there are at least two general ways to search for PLC. One can construct the ratio of the observed experimental cross section, σ_{exp}^{FSI}, (which of course includes FSI effects) to the calculated theoretical cross section without FSI, σ_{the}^{PW}:

$$T_{e/t}(Q^2) = \frac{\sigma_{exp}^{FSI}(Q^2, p_n)}{\sigma_{the}^{PW}(Q^2, p_n)} \tag{10}$$

where p_n is the neutron recoil momentum. Ideally, if PLC become more important with Q^2, then this ratio should tend toward unity as Q^2 increases (at fixed p_n). Unfortunately, this method requires low systematic uncertainties in both the experimental and theoretical cross sections. Since the expected effect for deuterium is quite small, this method is relatively impractical.

The ratio $T_{e/t}$ has been used for PLC search at SLAC [26] and Hall C [27]. Their data are shown in the top panel of Fig. 19 (red and blue points). One can see that the ratio is a) very close to one, b) independent of Q^2, and c) in agreement with the theoretical prediction for hadronic FSI (the dashed line). The conclusion is, there is no evidence of PLC in this data. Note that these data are expected to be very insensitive to the effects of PLC because the FSI contribution to the cross section at $p_n \leq 0.3$ GeV/c (see Fig. 13) is only 15%. The systematic uncertainties in the data and the calculation make it extremely difficult to find effects this small.

In order to increase the sensitivity of the measurement to the effects of PLC we do the following: (i) instead of looking at the ratio of experiment to theory (eq. 10) we use the ratios of experiment to experiment and theory to theory (Eqs. 3 and 4) which reduce the systematic uncertainties significantly, and (ii) we choose $\alpha = 1$ to increase the FSI contributions [15]. The effect of choosing $\alpha = 1$ is illustrated in Fig. 20, where the ratios of $d(e, e'p)n$ experimental and PWIA momentum distributions are shown with (red curve) and without (black curve) the $\alpha = 1 \pm 0.1$ cut. The FSI enhancements are seen in two momentum ranges: at $0.15 < p_n < 0.3$ GeV/c and $p_n > 0.35$ GeV/c, while at $p_n < 0.1$ GeV/c there is no change, since in this region FSIs are negligible.

Momentum spectra of recoil neutrons from the $d(e, e'p)n$ reaction with $\alpha_n = 1 \pm 0.1$ and $p_n < 1$ GeV/c are shown in Fig. 21. To calculate the $T_{e/e}$ ratios for each Q^2, we integrate the

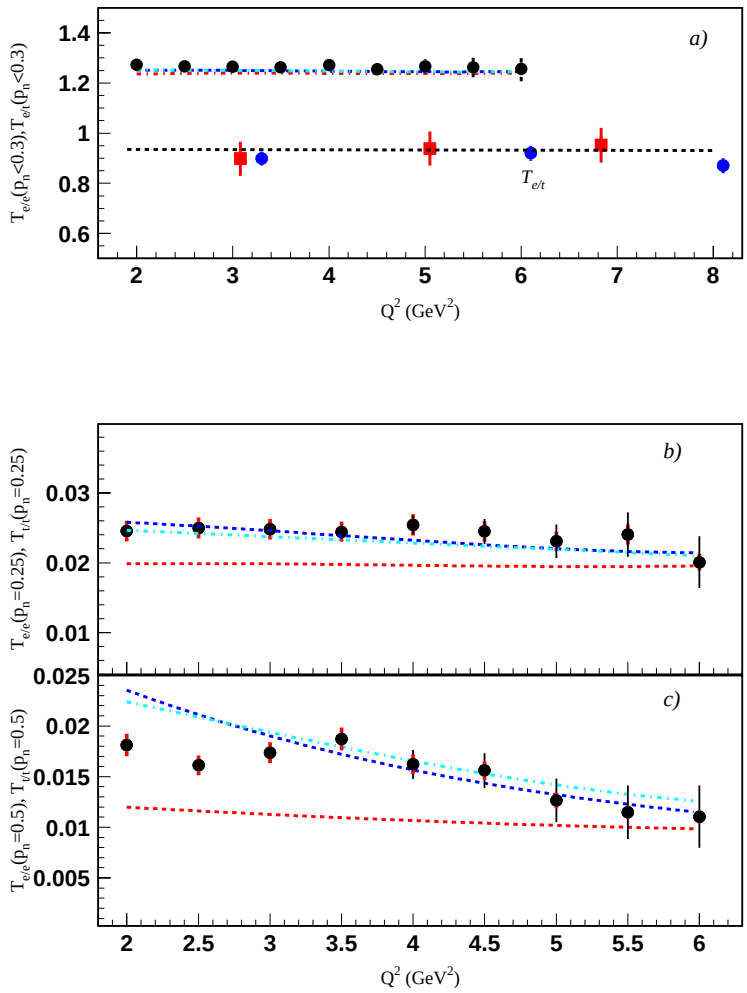

FIG. 19: **Top panel (a)**: *Lower points and curve:* The ratio $T_{e/t}$ of data to PWIA theory integrated over $p_n \leq 0.3$ GeV/c for data from SLAC (red points) and Hall C (blue points). The dashed line is the ratio of the calculations with and without FSI. *Upper points and curves:* The CLAS e6 ratio $T_{e/e}$ of the measured $d(e, e'p)n$ cross sections at $p_n \leq 0.3$ GeV/c and $p_n \leq 0.1$ GeV/c (points) and the corresponding theoretical ratios $T_{t/t}$ calculated for (NN) (red curve) and IC (blue and cyan curve) FSIs. The IC FSI calculations were carried out for two potentials in the deuterium WF, Paris (blue) and Argonne V18 (cyan). All three curves are very close to each other and hard to distinguish. **Middle panel (b)**: The CLAS e6 ratio $T_{e/e}$ of the measured $d(e, e'p)n$ cross sections at $0.2 \leq p_n \leq 0.3$ GeV/c and $p_n \leq 0.1$ GeV/c (points) and the same three theoretical ratios $T_{t/t}$ of the calculation in those two momentum ranges. **Bottom panel (c):** The CLAS e6 ratio $T_{e/e}$ of the measured $d(e, e'p)n$ cross sections at $0.4 \leq p_n \leq 0.6$ GeV/c and $p_n \leq 0.1$ GeV/c (points) and the same three ratios $T_{t/t}$ of the calculation in those two momentum ranges.

cross sections in four momentum ranges for each Q^2 bin. The resulting cross sections are shown

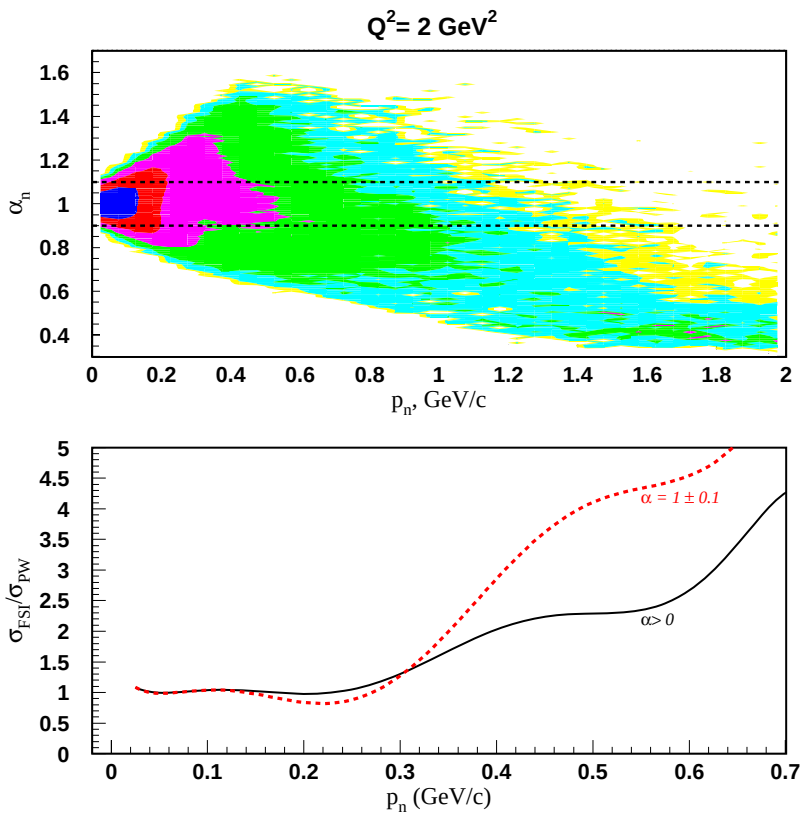

FIG. 20: Top panel: Cross section as a function of (α_n, p_n). The $\alpha_n = 1 \pm 0.1$ cut is shown by the horizontal lines. Bottom panel: the ratios of $d(e, e'p)n$ experimental and PWIA cross sections with (red curve) and without (black curve) the α_n cut. The FSI enhancements are seen in two momentum ranges: at $0.15 < p_n < 0.3$ GeV/c and $p_n > 0.35$ GeV/c.

in Fig. 22.

We attempt to replicate the SLAC and Hall C measurements in the $\alpha_n = 1 \pm 0.1$ kinematics, calculating the ratios $T_{e/e}$ and $T_{t/t}$ for CLAS e6 data by dividing the cross sections at $0 < p_n < 0.1$ GeV/c and $0 < p_n < 0.3$ GeV/c (see Fig. 21):

$$T_{e/e}(p_n < 0.3) = \frac{\sigma_{exp}(Q^2, p_n < 0.3)}{\sigma_{exp}(Q^2, p_n < 0.1)} \tag{11}$$

$$T_{t/t}(p_n < 0.3) = \frac{\sigma_{the}(Q^2, p_n < 0.3)}{\sigma_{the}(Q^2, p_n < 0.1)} \tag{12}$$

The resulting ratios are shown in the top panel of Fig. 19 (black points with corresponding theoretical curves). The ratios, although they have much lower uncertainties, also are independent of Q^2 and thus show no evidence of PLC.

In order to further increase the sensitivity of the PLC search, we restricted the integration region of $\sigma_{exp}^{FSI}(Q^2)$ to the region $0.2 \leq p_n \leq 0.3$ GeV/c (see Fig. 21), where the effects of FSI

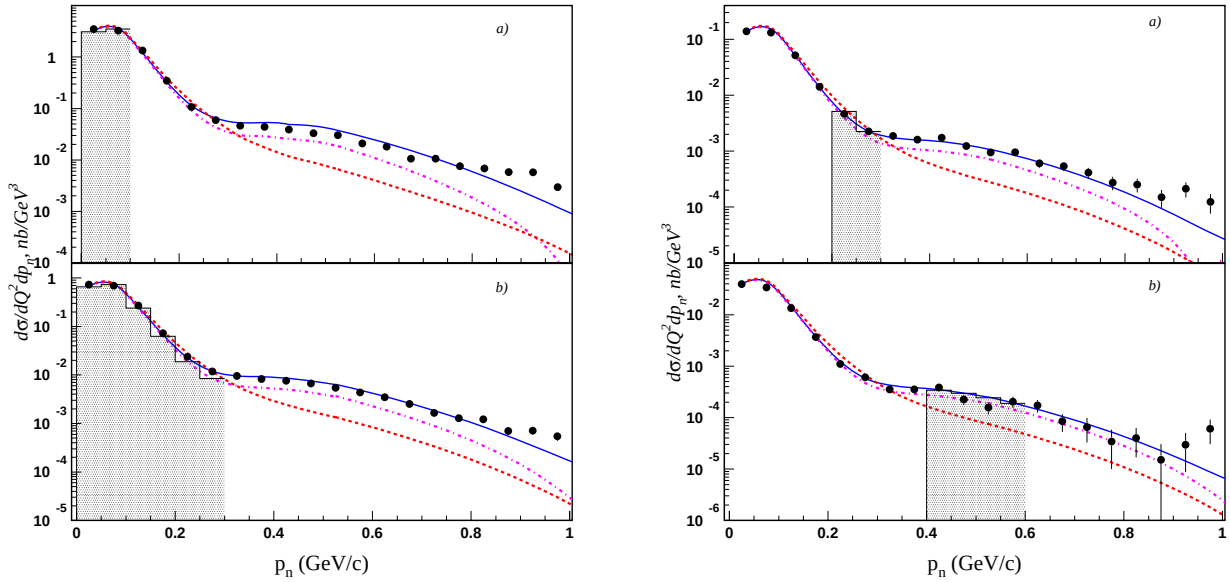

FIG. 21: $d(e,e'p)n$ reaction cross section vs neutron momentum in CLAS with $\alpha = 1 \pm 0.1$ cut. Left: (a) $Q^2 = 2$ and (b) 3, right: (a) 4 and (b) 5 GeV^2. The red (lowest) curves are PWIA, the magenta (intermediate) curves also include FSI, and the blue (highest) curves also include IC. The two curves for each reaction mechanism use the Paris and AV18 potentials.

are significantly greater so that

$$T_{e/e}(p_n = 0.25) = \frac{\sigma_{exp}(Q^2, 0.2 \leq p_n \leq 0.3)}{\sigma_{exp}(Q^2, p_n < 0.1)} \tag{13}$$

$$T_{t/t}(p_n = 0.25) = \frac{\sigma_{the}(Q^2, 0.2 \leq p_n \leq 0.3)}{\sigma_{the}(Q^2, p_n < 0.1)} \tag{14}$$

These results are shown in the middle panel of Fig. 19. $T_{e/e}$ has a small Q^2 dependence; however this is expected from the theoretical model since $T_{t/t}$ has the same Q^2 dependence.

In order to increase the sensitivity of the PLC search even further, we selected the region where FSI effects are maximum so that

$$T_{e/e}(p_n = 0.5) = \frac{\sigma_{exp}(Q^2, 0.4 \leq p_n \leq 0.6)}{\sigma_{exp}(Q^2, p_n < 0.1)} \tag{15}$$

$$T_{t/t}(p_n = 0.5) = \frac{\sigma_{the}(Q^2, 0.4 \leq p_n \leq 0.6)}{\sigma_{the}(Q^2, p_n < 0.1)} \tag{16}$$

(see Fig. 21). These results are shown in the bottom panel of Fig. 19. $T_{e/e}$ and $T_{t/t}$ have the same Q^2 dependence.

Thus, in the framework of J-M. Laget's diagrammatic appraoch, we obtain no evidence for the existence of PLCs at $Q^2 \leq 6$ GeV^2.

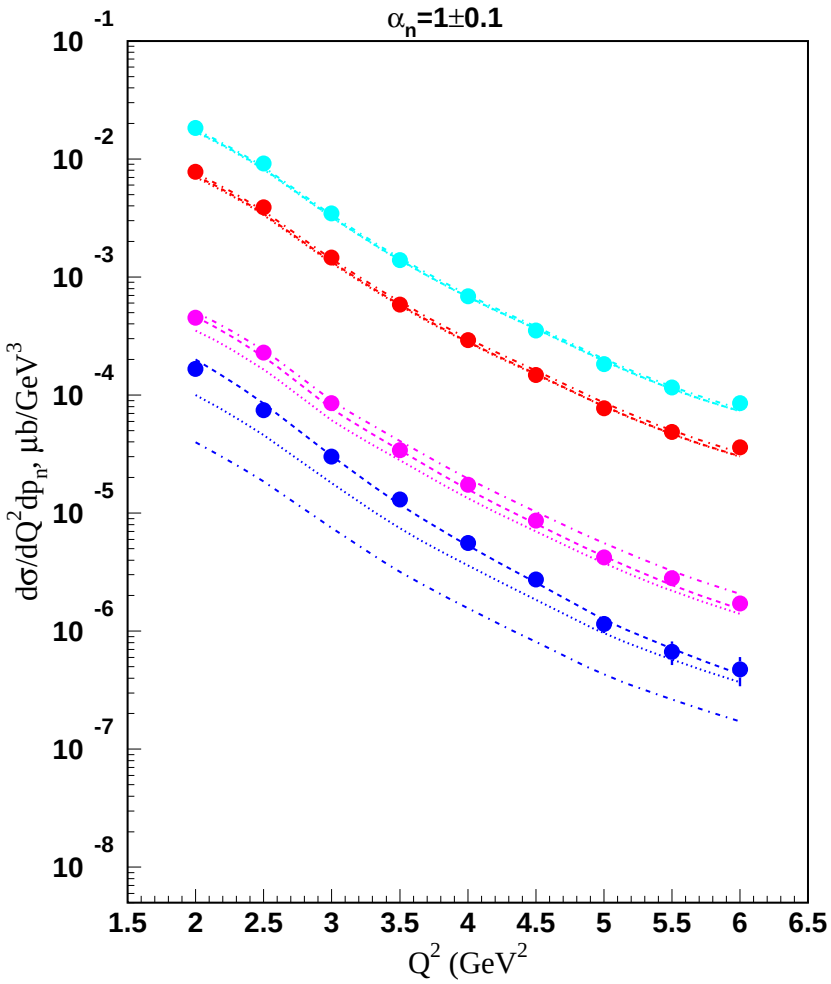

FIG. 22: $d(e,e'p)n$ reaction cross section vs Q^2 in four momentum intervals with $\alpha = 1 \pm 0.1$ cut. Red, cyan, magenta and blue are for $p_n \leq 0.1$, $p_n \leq 0.3$, $0.2 \leq p_n \leq 0.3$ and $0.4 \leq p_n \leq 0.6$ GeV/c, repectively. Curves are corresponding theoretical calculations: dash-dotted - PWIA, dotted - PWIA+NN, dash - full.

B. Previous searches for NM in deuterium

One direct signature for nucleon modification in nuclei is the change in the Q^2 dependence of the (eN_i) cross section, where N_i is a bound nucleon in a nucleus. Because nuclei are not just simple bags of non-interacting nucleons, there are certain probabilities that two or few nucleons can create short range correlations, and be in a deeply bound state (with momentum $p > 275$ MeV/c). Thus, in nuclei we can find the almost free (quasifree) non-interacting nucleons and also correlated, strongly interacting pairs (a few nucleonic clusters). It is obvious that there should be differences in the properties of these two nucleonic states. While nucleons in quasifree state should be (almost) unmodified, nucleons involved in SRC overlap and could be significantly modified. Therefore, to search for NM we should separate (eN_i) scattering in two regimes, a) where N_i is a deeply bound nucleon in an SRC and b) where N_i is quasifree (see Fig. 5). The

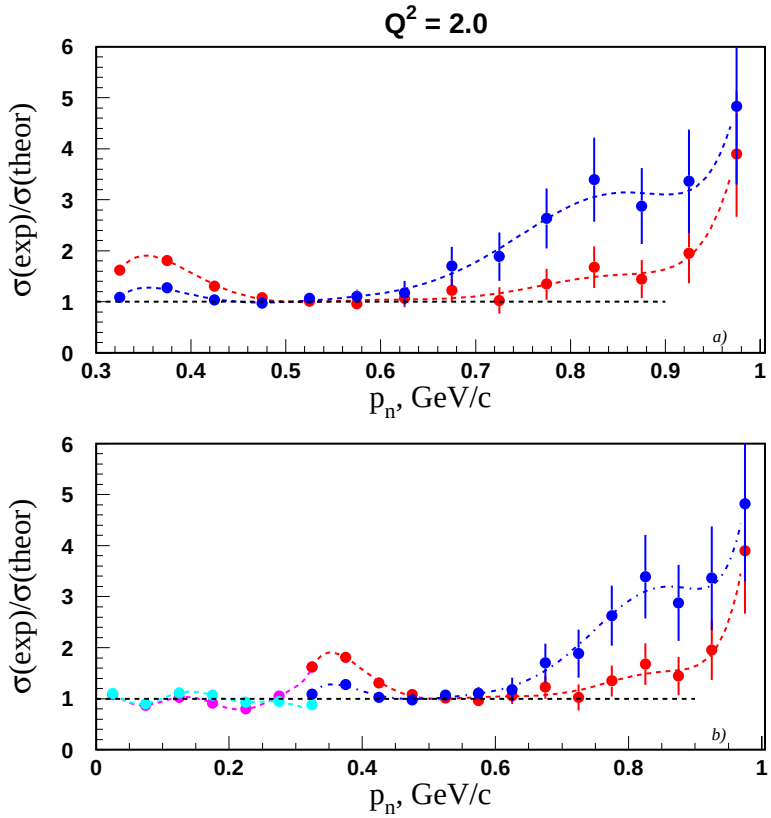

FIG. 23: a) The ratio of data to PWIA (red) and to the full calculation (blue) for $\alpha_n > 1.23$ at $Q^2 = 2$ GeV^2. Note that the horizontal scale starts at $p_n = 0.3$ GeV/c. b) The ratio of data to PWIA (magenta) and to the full calculation (cyan) for $\alpha_n = 1 \pm 0.1$ and $p_n < 0.3$ GeV/c at $Q^2 = 2$ GeV^2. The points at $p_n > 0.3$ GeV/c are identical to (a). The data are from CLAS e6.

problem is to separate nucleons belonging to these two states, especially to the NN SRC state where the probability is only 4% [1] in the deuterium wave function. Separation of this state in experiments like $d(e, e'p)n$ is an experimentally hard problem, since in the momentum range of the wave function where NN SRC are the main contribution, the FSI are also maximal.

Therefore, we need to find a kinematic region where the effects of FSI are suppressed and negligible. To do that, we look for a region in (α_n, p_n) space where the criteria of Eq. (7) ($\sigma_{exp} = \sigma_{PWIA} = \sigma_{FSI}(full)$) are satisfied.

We already know one region where this condition is satisfied. This is the region of $\alpha_n = 1 \pm 0.1$ and $p_n \leq 0.1$ GeV/c, (see Figs. 20 and 21 (left) a)) where the struck proton has low momentum and is not deeply bound *i.e.* is not modified.

In order to find a region where the proton has high momentum and is deeply bound, we will search the backward production kinematics (BPK), widely used in inclusive hadro- and lepto-production of backward hadrons (protons, pions, deuterons, etc.)[28, 29].

As a parameter of BPK we will use the light cone variable α_n (see Eq. (6)). We will choose $\alpha_n > \alpha_o$, with $\alpha_o > 1$, such that the criterion of Eq. (7) is satisfied in the $p_n > 300$ MeV/c region. α_o has been found experimentally to be $\alpha_o = 1.23$. For $\alpha_n > 1.23$ we found that

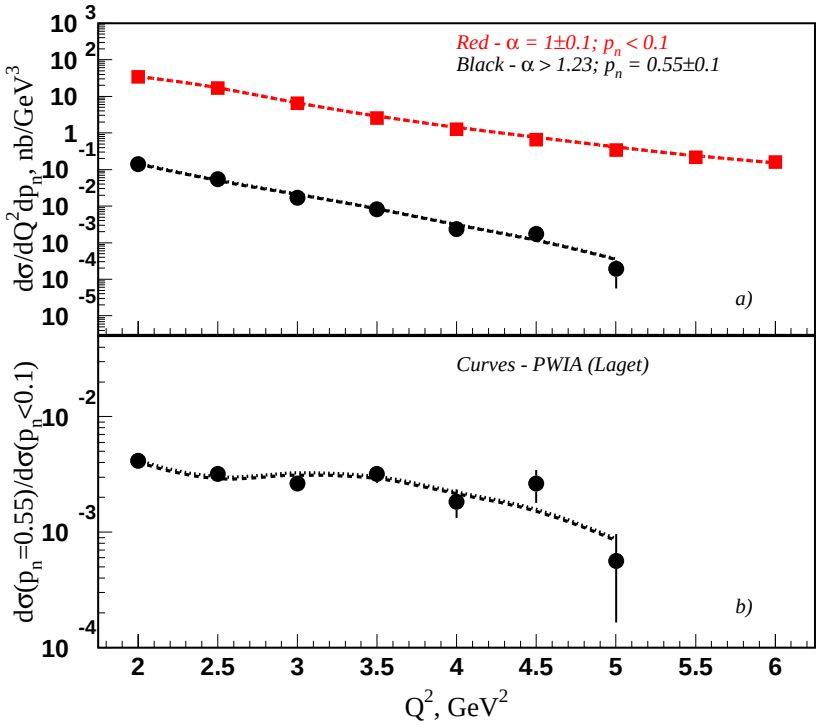

FIG. 24: a) The $d(e,e'p)n$ cross section vs Q^2. The red squares are for $p_n \leq 0.1$ GeV/c and $\alpha_n = 1\pm0.1$. The black circles are for $0.45 \leq p_n \leq 0.65$ GeV/c and $\alpha_m \geq 1.23$. The corresponding curves are the theoretical PWIA calculations. b) The ratio of the data at $0.45 \leq p_n \leq 0.65$ GeV/c and $\alpha_m \geq 1.23$ to the data at $p_n \leq 0.1$ GeV/c and $\alpha_n = 1 \pm 0.1$. The curve is the ratio of the PWIA calculations. The data are from CLAS e6.

criterion Eq.(7) is satisfied for $0.45 \leq p_n \leq 0.65$ GeV/c only. This is shown in Fig. 23a, where the ratios of the experimental momentum distribution to PWIA (red) and to the full calculation (blue) are presented. One can see that these ratios at $0.45 \leq p_n \leq 0.65$ GeV/c are equal to each other and to unity, which means that the FSI contribution is negligible.

Now we have two neutron momentum regions, ($p_n < 0.1$ GeV/c, at $\alpha_n = 1 \pm 0.1$) and ($0.45 \leq p_n \leq 0.65$ GeV/c, at $\alpha_n > 1.23$), where FSIs are negligible (see Fig. 23b), *i.e.* the $d(e,e'p)n$ cross section is proportional to the deuterium wave function only.

By studying the Q^2-dependence of the ratio of the measured cross section in these two regions and comparing this ratio with the same ratio calculated in PWIA, where the struck nucleon form factors are similar for both momentum ranges, we can hope to see evidence for differences in the electron interaction with the struck proton. Differences in the experimental and theoretical cross section ratios will provide evidence for modification of the deeply bound proton.

The experimental and theoretical PWIA cross sections and ratios are shown in Fig. 24. Although the ratio of the data decreases with Q^2, so does the ratio of the PWIA cross sections.

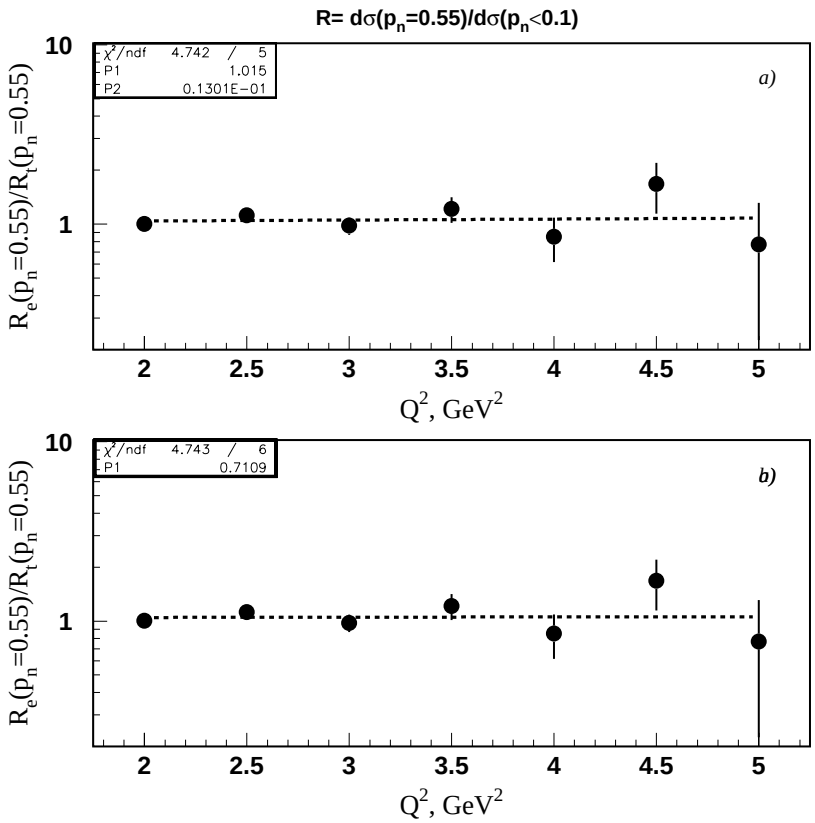

FIG. 25: a, b) The double ratio $T_{e/e}/T_{t/t}$ of the ratios of the $d(e,e'p)n$ cross section at $0.45 \leq p_n \leq 0.65$ GeV/c and $\alpha_m > 1.23$ to the cross section at $p_n \leq 0.1$ GeV/c and $\alpha_n = 1 \pm 0.1$ relative to the same ratio of the PWIA cross sections. The curves in a) and b) are a linear fit and a dipole form factor fit (Eq. 18), respectively.

The double ratio $T_{e/e}/T_{t/t}$ of the experimental ratio to the PWIA ratio is shown in Fig. 25. There is no evidence for any nucleon modification. A straight line fit to the double ratio yields a slope of 0.01 ± 0.08 $(\mathrm{GeV}^2)^{-1}$ (see Fig. 25a). In the framework of the diagramatic approach there is no evidence for any nucleon modification.

This data also provides reasonably stringent limits on nucleon modification. The simplest model of a distorted nucleon uses the dipole form factor with a different radius:

$$FF_{nm} = \frac{1}{\left(1 + \frac{Q^2}{r}\right)^2} \tag{17}$$

In this model, the double ratio $T_{e/e}/T_{t/t}$ would be

$$\frac{T_{e/e}}{T_{t/t}} = \frac{1/\left(1 + \frac{Q^2}{r}\right)^4}{1/\left(1 + \frac{Q^2}{0.7\mathrm{GeV}^2}\right)^4} \tag{18}$$

When we fit r to this data, we get $r = 0.71 \pm 0.01$ GeV^2 (see Fig. 25b).

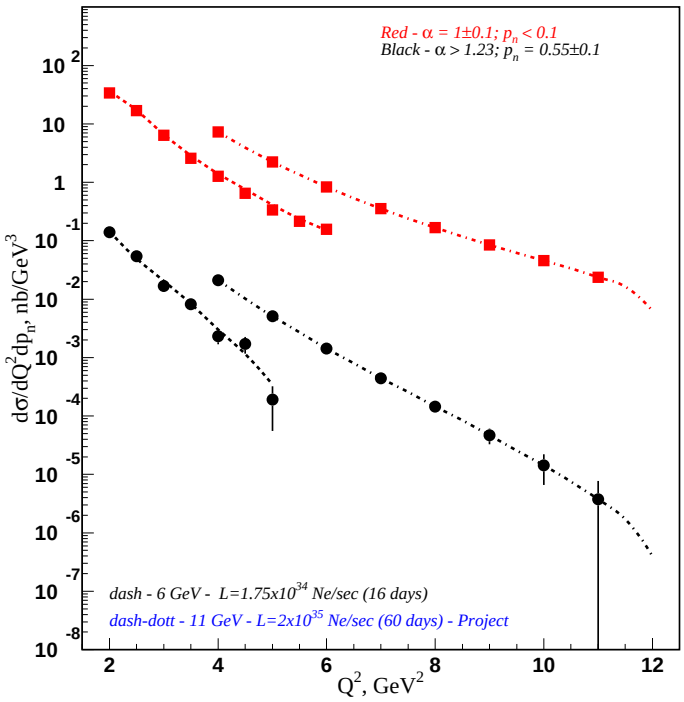

FIG. 26: Statistical precision of the cross section measurements for the nucleon modification search at $\alpha_n = 1 \pm 0.1$ and $p_n \leq 0.1$ GeV/c (black lower curves) and at $\alpha_n \geq 1.23$ and $0.45 \leq p_n \leq 0.65$ GeV/c (red upper curves) as a function of Q^2. The data from the existing e6 measurement extend from $Q^2 = 2$ to 5 GeV^2 and the data from the proposed measurement extend up to $Q^2 = 11$ GeV^2.

C. Expected results with the CLAS12

The main feature of the proposed CLAS12 study is that all procedures and methods as well as theoretical calculations were already successfully used in previous e6 measurements and calculations. As in the e6 case, in the proposed study we will analyze the ratios of cross sections measured in four kinematic ranges

- $p_n \leq 0.3$ GeV/c, and $\alpha_n = 1 \pm 0.1$.
- $0.2 \leq p_n \leq 0.3$ GeV/c, and $\alpha_n = 1 \pm 0.1$.
- $0.4 \leq p_n \leq 0.6$ GeV/c, and $\alpha_n = 1 \pm 0.1$.
- $0.45 \leq p_n \leq 0.65$ GeV/c, and $\alpha_n > 1.23$

to the cross section measured at $p_n \leq 0.1$ GeV/c, and $\alpha_n = 1 \pm 0.1$.

In order to estimate the expected statistics, we extrapolated from the e6 cross sections in those kinematic ranges measured with CLAS at a beam energy of 5.7 GeV. The extrapolation involves the following elements:

- luminosity increased from $2 \cdot 10^{34}$ to $2 \cdot 10^{35} N \cdot e$ /(cm^2-s)
- beam energy increased from 5.7 to 11 GeV

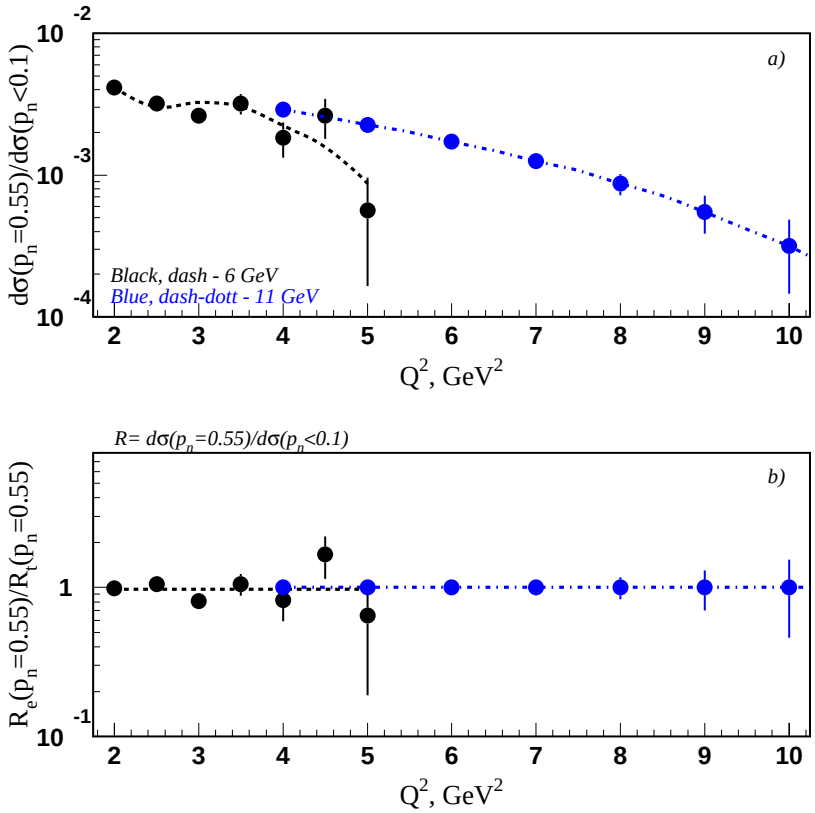

FIG. 27: Statistical precision of the expected results for the nucleon modification search. The upper plot shows the ratio of the cross section measured at $\alpha_n \geq 1.23$ and $0.45 \leq p_n \leq 0.65$ GeV/c to that measured at $\alpha_n = 1 \pm 0.1$ and $p_n \leq 0.1$ GeV/c as a function of Q^2. The black points and black dashed curve is the existing e6 data. The blue points and dash-dot curve are the expected results of this measurement. The lower plot shows the double ratio of the experimental ratio to theory ratio.

- CLAS geometrical acceptance unchanged
- beam time increased from 16 to 32 days

Nucleon modification search: The nucleon modification search involves calculating the ratio, $T_{e/e}$, of the $d(e,e'p)n$ cross section measured at $\alpha_n > 1.23$ and $0.45 \leq p_n \leq 0.65$ GeV/c to that measured at $\alpha_n = 1 \pm 0.1$ and $p_n \leq 0.1$ GeV/c as a function of Q^2 and comparing that to the calculated theoretical ratio, $T_{t/t}$. The expected statistical precision of the cross section measurements in those regions is shown in Fig. 26. Note that the proposed measurement will greatly increase both the statistical precision of the existing measurements at $Q^2 \leq 5$ GeV^2 and the Q^2 range of the measurements. The expected precision of the experimental ratios is shown in Fig. 27a and the expected precision of the double ratio of $T_{e/e}/T_{t/t}$ is shown in Fig. 27b. These data will significantly constrain nucleon modification models up to $Q^2 = 8$ GeV^2 and will provide less precise data up to $Q^2 = 10$ GeV^2.

Point-Like Configuration search: The PLC search involves calculating the three ratios, $T_{e/e}$, of the $d(e,e'p)n$ cross section measured at the three regions of neutron momentum, $p_n \leq 0.3$ GeV/c, $0.2 \leq p_n \leq 0.3$ GeV/c,and $0.4 \leq p_n \leq 0.6$ GeV/c to that measured at $p_n \leq 0.1$ GeV/c

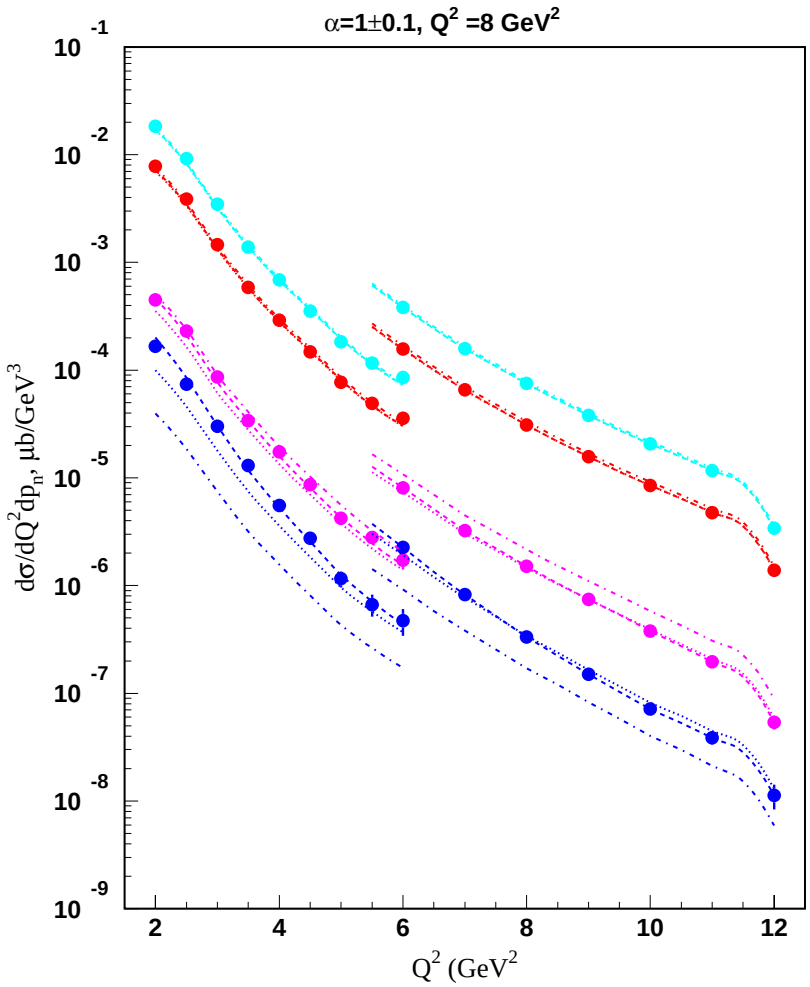

FIG. 28: Statistical precision of the $d(e,e'p)n$ cross section measurements for the Point-Like Configuration (PLC) search for the four kinematic regions. **Left side** ($Q^2 \leq 6$ GeV^2): The existing CLAS e6 data and corresponding theoretical calculations, **Right side** ($Q^2 \geq 6$ GeV^2): The projected CLAS12 data and corresponding theoretical calculations. *Points and curves*: Red, cyan, magenta and blue - for momentum ranges $p_n < 0.1$ GeV/c, $p_n < 0.3$ GeV/c, $0.2 < p_n < 0.3$ GeV/c and $0.4 < p_n < 0.6$ GeV/c respectively. *Curves*: Dash-dotted, dotted and dashed are PWIA, PWIA+NN and full calculations. The data from the existing e6 measurement extend from $Q^2 = 2$ to 6 GeV^2 and the data from the proposed measurement extend up to $Q^2 = 12$ GeV^2.

as a function of Q^2 and comparing that to the corresponding calculated theoretical ratios, $T_{t/t}$. The expected statistical precision of the cross section measurements in those regions is shown in Fig. 28. Note that the proposed measurement will greatly increase both the statistical precision of the existing measurements at $Q^2 \leq 5$ GeV^2 and the Q^2 range of the measurements.

The expected statistical precision of the ratios is shown in Fig. 29. Note the proposed measurement will greatly increase the statistical precision of the ratios at $4 \leq Q^2 \leq 6$ GeV^2 and it will extend the measurements out to $Q^2 = 12$ GeV^2. The solid magenta points show the expected ratios in the absence of any PLC effects and the open points show the expected

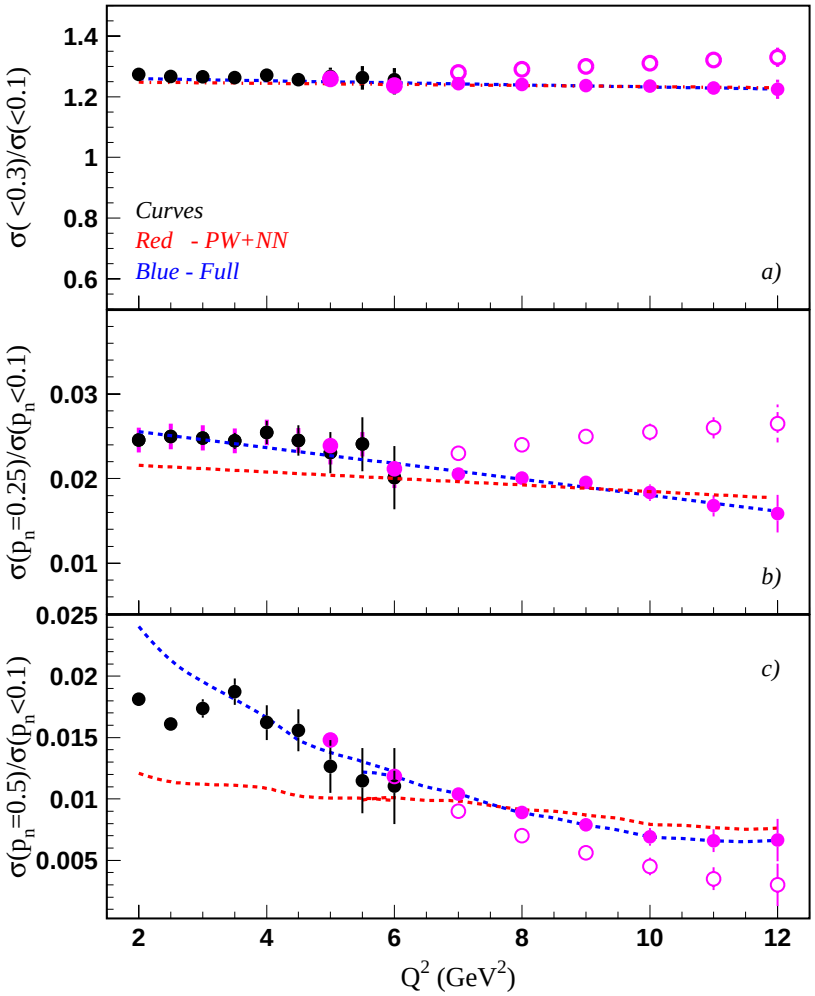

FIG. 29: Statistical precision of the expected results for the PLC search for three kinematics. The black points are the existing CLAS e6 data. The magenta points are the expected results of CLAS12 measurement. *Curves*: $T_{t/t}$ with PWIA+NN (red) and with full (blue) calculations. The solid magenta points show the expected ratios in the absence of any PLC effects and the open points show the expected ratios for the PLC effects. a) the ratio of the cross section measured at $p_n \leq 0.3$ GeV/c to that measured at $p_n \leq 0.1$ GeV/c as a function of Q^2. b) the ratio of the cross section at $0.2 \leq p_n \leq 0.3$ GeV/c to the cross section at $p_n \leq 0.1$ GeV/c as a function of Q^2. c) the ratio of the cross section at $0.4 \leq p_n \leq 0.6$ GeV/c to the cross section at $p_n \leq 0.1$ GeV/c as a function of Q^2.

ratios for the PLC effects, which were found using the predictions of Ref. [6] after shifting (just by hand) the onset of PLC starting from $Q^2 \approx 3$ GeV^2 to $Q^2 = 7$ GeV^2. The goal of showing these points is to demonstrate the **direction** (not value) of changes, if PLC have a sizable

contribution.

V. SUMMARY

1. The exclusive $d(e, e'p)n$ reaction at high Q^2 is an excellent channel to investigate the short range properties of nucleons.

2. Existing CLAS e6 data and corresponding thereotical calculations demonstrate that the mechanism of this reaction can be well controlled up to $Q^2 = 6$ GeV^2 for $p_n \leq 0.75$ GeV/c.

3. In the framework of the CLAS e6 program two search programs have been completed:

   - Search for Point Like Configuration (PLC) predicted in QCD, and
   - Search for deeply bound nucleon modification (NM) in deuterium

   There is no evidence for either PLC or NM at $Q^2 \leq 6$ GeV^2 in the framework of the theoretical diagramatic approach.

   Therefore new measurements at higher Q^2 are needed.

4. The continuation of these investigations is proposed up to $Q^2 = 12$ GeV^2 using CLAS12.

5. It is shown that the experimental acceptances and resolutions of CLAS12 will be quite acceptable for the proposed studies.

6. The expected experimental data will allow us to search for

   - Point-like configurations (PLC) in the proton wave function (predicted by QCD) and
   - Modification of deeply bound nucleons (nucleons involved in SRC at momenta $p = 0.55 \pm 0.1$ GeV/c)

   in the highest available Q^2 range, up to 12 GeV^2

7. Projected CLAS12 luminosity will provide sufficient statistics with 32 days beam time to complete the proposed physics program

VI. INSITUTIONAL COMMITMENT TO CLAS12

The Yerevan Physics Insitute group is actively involved in this proposal, as well as several other proposals using CLAS12. Among CLAS12 baseline equipment, the group is participating in the upgrade of the Electromagnetic Calorimeter. This includes designing, prototyping, constructing, calibrating and commissioning the EC Preshower detector (under the supervision of S. Stepanyan). It also includes the writing and implementing the EC Preshower software package. Three faculty or staff members and several graduate students are likely to work at least part time on this project in the next few years.

The Old Dominion University group is actively involved in this proposal, as well as several other proposals using CLAS12. Other members of our group are pursuing a proposal for Hall A, but their contributions are not included here.

Among CLAS12 baseline equipment, the group intends to take responsibility for the design, prototyping, construction and testing of the Region 1 Drift Chamber. Five faculty (including one research faculty) and one technician are likely to work at least part time on this project in the next few years. Funding for the group is from DOE and from the university (75% of research faculty salary + one regular faculty summer salary + 50% of the technician).

The university has also provided 6000 square feet of high bay laboratory space with clean room capabilities for our use. We will seek other sources of funding as appropriate.

Gail Dodge is the chair of the CLAS12 Steering Committee and the user coordinator for the CLAS12 tracking technical working group.

Beyond the baseline equipment, the group is also interested in exploring improvements to the BoNuS detector and a future RICH detector for CLAS12.

---

[1] K. Egiyan *et al.*, Phys. Rev. Lett. **96**, 082501 (2006).
[2] http://www.jlab.org/exp_prog/proposals/94/PR94-019.pdf
[3] K. Egiyan, *et al.*, in preparation.
[4] A. V. Klimenko *et al.*, Phys. Rev. C **73**, 035212 (2006) [arXiv:nucl-ex/0510032].
[5] L.L. Frankfurt and M.I. Strikman, Nucl.Phys., **B250**, 143 (1985)
[6] L.L. Frankfurt, W.R. Grinberg, G.A. Miller, M.M. Sargsian, and M.I.Strikman, Z.Phys. **A 352**, 97 (1995).
[7] G. van der Steenhoven *et al.*, Phys. Rev. Lett., **58**, 1727, (1987).
[8] P. Ulmer *et al.*, Phys. Rev. Lett., **59**, 2259, (1987).
[9] D. Reffay-Pickeroen *et al.*, Phys. Rev. Lett., **60**, 776, (1988).
[10] T.D. Cohen, J.W. Van Orden, and A. Picklesimer, Phys. Rev. Lett., **59**, 1267, (1987).
[11] S. Strauch *et al.*, Phys. Rev. Lett., **91**, 052301, (2003).
[12] R. Schiavilla *et al.*, Phys. Rev. Lett., **94**, 072303, (2005).
[13] B.A. Mecking *et al.*, Nucl. Instrum. Methods Phys. Res. A
[14] K. Egiyan *et al.*, CLAS-Note. (2006)
[15] M.M. Sargsian *et al.*, J.Phys. **G29**, R1 (2003).
[16] J.-M. Laget, Phys. Lett. **B609**, 49 (2005).
[17] J.M. Laget, Phys. Rep. **69**, 1 (1981).
[18] J.M. Laget, Nucl. Phys.**A579**, 333 (1994).
[19] M. Lacombe *et al.*, Phys. Lett. **B101**, 139 (1981).
[20] O. Gayou *et al.*, Phys. Rev. Lett. **88**, 092301 (2002).
[21] S. Galster *et al.*, Nucl. Phys. **B32**, 221 (1971).

[22] V.V. Frolov *et al.*, Phys. Rev. Lett. **82**, 45 (1999).
[23] M. Ungaro *et al.*, to be submitted and private communication.
[24] L.L. Frankfurt, M.M. Sargsian and M.I. Strikman, Phys. Rev. C **56**, 1124 (1997).
[25] J.M. Laget, in: *Workshop on Color Transparency (CT97)*, ed. E. Voutier, Grenoble 1997. http://isnpx0162.in2p3.fr/polder/ct97/Jlag/Jlag.html.
[26] T.G. O'Neill et al., Phys.Lett B **351** 87 (1995).
[27] K. Garrow et al., Phys. Rev. C **66** 044613 (2002).
[28] L.L. Frankfurt and M.I. Strikman, Phys. Rep. **76**, 215 (1981).
[29] L.L. Frankfurt and M.I. Strikman, Phys. Rep. **160**, 235 (1988).